# PV CELL TEMPERATURE ESTIMATION AND PERFORMANCE ANALYSIS BASED ON CHANGING ENVIRONMENTAL EFFECTS

A THESIS SUBMITTED TO
THE BOARD OF GRADUATE PROGRAMS
OF
MIDDLE EAST TECHNICAL UNIVERSITY, NORTHERN CYPRUS CAMPUS

BY

YOUSSEF MAGED MOHAMED BALIGH YOUSSEF

IN PARTIAL FULFILLMENT OF THE REQUIREMENTS
FOR
THE DEGREE OF MASTER OF SCIENCE
IN SUSTAINABLE ENVIRONMENT AND ENERGY SYSTEMS PROGRAM

AUGUST 2022

Approval of the Board of Graduate Programs

Prof. Dr. Cumali Sabah
Chairperson

I certify that this thesis satisfies all the requirements as a thesis for the degree of Master of Science

Assoc. Prof. Dr. Ceren İnce Derogar
Program Coordinator

This is to certify that we have read this thesis and that in our opinion it is fully adequate, in scope and quality, as a thesis for the degree of Master of Science.

Asst. Prof. Dr. Canraş Batunlu
Supervisor

**Examining Committee Members**

| | | |
|---|---|---|
| Asst. Prof. Dr. Canraş Batunlu | Electrical and Electronics Engineering, METU NCC | |
| Asst. Prof. Dr. Bertuğ Akıntuğ | Civil Engineering, METU NCC | |
| Asst. Prof. Dr. Ali Serener | Electrical and Electronics Engineering, NEU | |

**I hereby declare that all information in this document has been obtained and presented in accordance with academic rules and ethical conduct. I also declare that, as required by these rules and conduct, I have fully cited and referenced all material and results that are not original to this work.**

Name, Last Name: Youssef Maged Mohamed Baligh, Youssef

Signature:

## ABSTRACT

### PV CELL TEMPERATURE ESTIMATION AND PERFORMANCE ANALYSIS BASED ON CHANGING ENVIRONMENTAL EFFECTS

Youssef, Youssef Maged Mohamed Baligh
Master of Science, Sustainable Environment and Energy Systems Program
Supervisor: Asst. Prof. Dr. Canraş Batunlu

August 2022, 111 pages

Climate change effects are on the rise due to greenhouse gas emission from the combustion of fossil fuels. The need to find alternative sustainable and renewable energy sources is of great importance. In Northern Cyprus, solar energy resources are abundant and must be utilized to provide energy security for the future and mitigate the effects of climate change. Photovoltaic (PV) solar panels are used to harness solar energy and produce electricity. The operating cell temperature of PV modules directly affects the overall performance of PV systems. Lower operating cell temperatures result in a higher module efficiency and therefore higher energy generation. Accurate estimation of the PV cell temperature is crucial to accurately assess the feasibility and economic viability of a PV power plant project. Several PV cell temperature estimation models are presented in the literature and are used in different applications for cell temperature estimation. PV cell temperature estimation models are investigated to assess the performance and reliability of the models specifically for Northern Cyprus weather conditions. Furthermore, environmental factors such as dust affect the performance of PV modules as dust layers cause the attenuation of sunlight which prevent the utilization of incident solar radiation by the PV modules. The accumulation of dust on PV modules is called soiling. The effect of soiling on the performance of PV modules is investigated.



Keywords: PV Cell Temperature Estimation, Soiling of PV Modules, Solar Energy

# ÖZ

## DEĞIŞEN ÇEVRESEL ETKILERE DAYALI FOTOVOLTAİK HÜCRE SICAKLIK TAHMİNİ VE PERFORMANS ANALIZI

Youssef, Youssef Maged Mohamed Baligh
Yüksek Lisans, Sürdürülebilir Çevre ve Enerji Sistemleri
Tez Yöneticisi: Asst. Prof. Dr. Canraş Batunlu

Agustos 2022, 111 sayfa

Fosil yakıtların yanmasından kaynaklanan sera gazı emisyonu nedeniyle, iklim değişikliği üzerindeki etkiler artmaktadır. Alternatif, sürdürülebilir ve yenilenebilir enerji kaynakları bulma ihtiyacı büyük önem taşımaktadır. Kuzey Kıbrıs'ta güneş enerjisi kaynakları çok miktarda mevcuttur ve gelecek için enerji güvenliğini sağlamak ve iklim değişikliğinin etkilerini azaltmak için kullanılmalıdır. Fotovoltaik (PV) güneş panelleri, güneş enerjisini kullanmak ve elektrik üretmek için kullanılır. PV modüllerinin çalışma hücresi sıcaklığı, PV sistemlerinin genel performansını doğrudan etkiler. Daha düşük çalışma hücresi sıcaklıkları, daha yüksek modül verimliliği ve dolayısıyla daha yüksek enerji üretimi ile sonuçlanır. Bir PV enerji santrali projesinin fizibilitesini ve ekonomik uygulanabilirliğini doğru bir şekilde değerlendirmek için PV hücre sıcaklığının doğru tahmini çok önemlidir. Literatürde çeşitli PV hücre sıcaklık tahmin modelleri sunulmaktadır ve hücre sıcaklığı tahmini için farklı uygulamalarda kullanılmaktadır. PV hücre sıcaklık tahmin modelleri, özellikle Kuzey Kıbrıs hava koşulları için modellerin performansını ve güvenilirliğini değerlendirmek için araştırılmıştır. Ayrıca, toz katmanları güneş ışığının zayıflamasına neden olduğundan, güneş ışınımının PV modülleri tarafından kullanılmasını engellediği için, toz gibi çevresel faktörler PV modüllerinin performansını etkiler. PV modüllerinde toz birikmesine kirlenme denir. Kirlenmenin PV modüllerinin performansı üzerindeki etkisi de tez içerisinde araştırılmıştır.

Anahtar Kelimeler: Fotovoltaik Hucre Sicaklik Hesabi, Fotovoltaik Modullerin Tozlanmasi, Gunes Enerjisi

***To my beloved mother, without whom I would not be who I am today.***

## ACKNOWLEDGMENTS

Firstly, I would like to express my deepest gratitude to my thesis advisor Asst. Prof. Dr. Canraş Batunlu for his constant support, patience, and understanding throughout the whole study period. Without his help and guidance, it would have not been possible to complete this research.

I would like to thank Assoc. Prof. Dr. Onur Taylan for the extensive knowledge I learned through him and continue to benefit from since my undergraduate years. Without his teachings it would have been much harder to continue the journey of graduate studies.

I would like to thank Assoc. Prof. Dr. Ceren İnce Derogar for her support and understanding throughout my whole postgraduate study period. I would also like to extend my thanks to Prof. Dr. Murat Fahrioğlu, and Asst. Prof. Dr. Bertuğ Akıntuğ for their valuable contributions to my understanding of renewable energy and sustainability. Without them there would be no SEES department.

Last but not least, I would like to thank all my family and friends for their continuous love, support, and encouragement. Without their presence life would no longer hold any meaning.

## TABLE OF CONTENTS

## LIST OF TABLES

TABLES

## LIST OF FIGURES

FIGURES

# CHAPTER 1

# INTRODUCTION

Over the last few decades, due to the recent advancement in technologies and increasing population, the demand for energy has increased drastically causing the rapid depletion of fossil fuel energy sources. Other than the depletion of fossil fuels, climate change effects are on the rise mainly due to greenhouse gas emission from the combustion of fossil fuels. Climate change effects include loss of life and vegetation, droughts, floods, scarcity of food and water, extreme weather, and other forms of economic loss. For these reasons, the need to find alternative sustainable and renewable energy sources is of great importance. The availability of clean energy is crucial for the sustainable development of humanity and has an effect on all three pillars of sustainability which are economic viability, the protection of the environment, and social equity.

Renewable energy is basically energy that is derived from resources that are replenished at a rate faster than the rate it is consumed. Examples of renewable energy resources include sunlight, wind, hydroelectric, geothermal, biomass, hydrogen, and ocean energy. Renewable energy is generally considered sustainable because it is naturally replenished on a human timescale in addition to it being a clean source of energy. Clean energy implies energy that is derived from renewable energy sources that do not pollute the atmosphere and have zero emissions of greenhouse gases such as carbon dioxide. Clean energy sources have little to no negative environmental impacts. One of the main goals of sustainable development proposed by the United Nations is to develop affordable and clean energy.

In Northern Cyprus, solar energy resources are abundant and must be utilized in order to provide energy security for the future and mitigate the effects of climate change. **Figure 1.1** shows a solar resource map for Cyprus by The World Bank

Group. It is observed from the solar resource map that Morphou which is also known as Güzelyurt has one of the highest photovoltaic power potentials in Cyprus. This is where METU NCC is located and more specifically the METU NCC solar power plant.

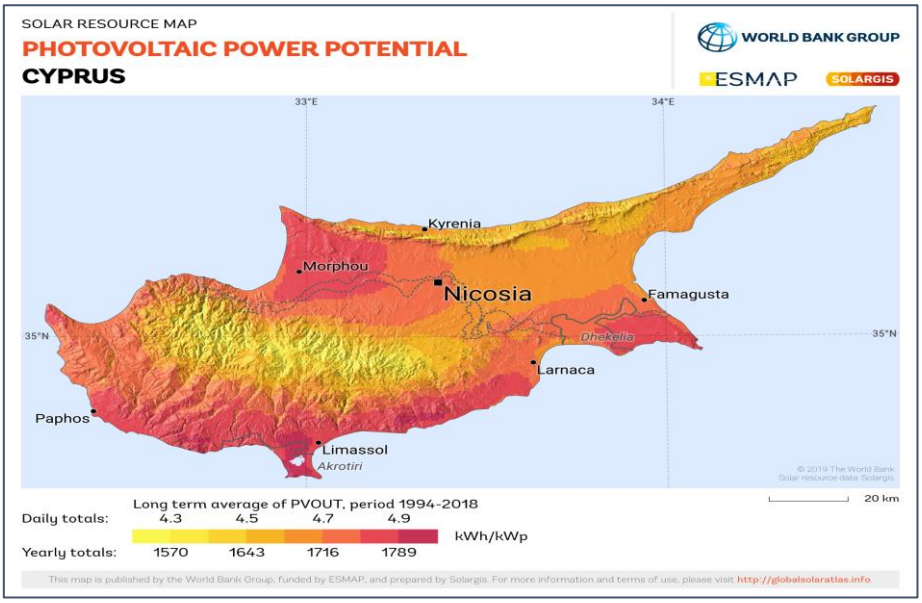


Figure 1.1 Photovoltaic power potential solar resource map for Cyprus (World Bank Group, 2022)

Photovoltaic (PV) solar modules are used to harness solar energy and produce electricity. The operating cell temperature of PV modules directly affects the overall performance of PV systems. Lower operating cell temperatures result in a higher module efficiency and therefore higher energy generation. For this reason, the accurate estimation of the PV operating cell temperature is crucial to assess the feasibility and economic viability of a PV power plant project and therefore plays a significant role in encouraging stakeholders and investors to invest in solar energy projects.

Several PV cell temperature estimation models are developed in the literature and are used to estimate the operating cell temperature of PV modules under different climatic conditions. The suitability of a model in predicting the PV cell temperature may be in question when the conditions at hand are different from the conditions

assumed when the model was developed. In this thesis, multiple models from the literature are investigated to find the most accurate model in predicting the PV cell temperature for Northern Cyprus weather conditions and more specifically for the METU NCC power plant. The accuracy of the PV cell temperature predictions is assessed by comparing it to actual PV cell temperature measurements. The most accurate prediction models with the lowest errors can then be used to evaluate future PV projects in the region more accurately.

Finally, outdoor PV installations are subject to dust accumulation or in other words soiling. The soiling of PV modules has a significant effect on its performance and its degradation as dust layers cause the attenuation of sunlight from the PV modules. The rate at which dust layers are formed on the surface of the module is determined by the surrounding environment, climatic conditions, and the type of installation of the PV module. Furthermore, the chemical and physical properties play an important role in determining the amount of sunlight attenuation caused by the dust layers. Different environments have different types of dust and different climates therefore the effect of soiling on the performance of PV modules differs from location to location. A PV soiling study is conducted in this thesis to find its effect on the performance of PV modules in the Northern Cyprus weather conditions.

# CHAPTER 2

# LITERATURE REVIEW

In this chapter the literature review is presented. It is divided into three main parts. First, the PV cell temperature estimation methods found in the literature are presented along with the prediction models. Next, the PV cell temperature measurement methods are presented. Finally, studies regarding the effect of soiling on the performance of PV modules are presented.

## 2.1 PV Cell Temperature Estimation Methods

Estimating the PV cell temperature is very important in order to be able to predict the energy generation of a PV power plant. It is used to assess the long-term performance of PV modules and find the module's efficiency which is dependent on the PV cell temperature. If the PV cell reaches a high temperature the efficiency of the module drops. This is because the cell temperature affects the I-V characteristics of the module and consequently as the cell temperature rises the power output decreases (Mattei et al., 2006). The PV cell temperature depends on several variables such as the PV technology type, materials used in the encapsulation, the configuration/installation of the modules, and climatic conditions (including the ambient temperature, incident solar irradiation, wind speed, and shading) (Alonso García & Balenzategui, 2004).

Different models have been developed in order to predict the PV cell temperature using mainly the ambient temperature, solar irradiance, and in some models the wind speed. The challenge here lies in the fact that each model has been developed under specific conditions. When the conditions vary significantly from the conditions specified by a model, the accuracy of the model may be in question (Muzathik,

2014). It was observed from the literature that the best way to predict the PV cell temperature is through developing a model according to each specific case's environmental conditions. If not possible, then some models may be appropriate and are able to predict the PV cell temperature within an acceptable error range. The suitability of a PV cell temperature estimation method may differ from region to region according to the climatic conditions and its similarity to the testing conditions and assumptions made during the development of the model.

Another consideration to bear in mind when choosing an appropriate PV cell temperature estimation model is wind speed. Wind speed has a significant effect on the PV cell temperature as it provides cooling for the module. It is essential to consider it although standard approaches have been developed without considering wind as a factor. It was found by Schwingshackl et al. (2013) that models that include wind data in PV cell temperature predictions performed better than standard approaches that did not include wind. Several models that are widely used in the literature are presented in the following sections.

### 2.1.1 Nominal Operating Cell Temperature (NOCT) Method

The Nominal Operating Cell Temperature (NOCT) model is the most commonly used standard approach to predict PV cell temperature. $T_{NOCT}$ is the nominal operating cell temperature of a PV module at the standard test conditions of $T_{a,NOCT} = 20\ °C$ (ambient temperature), $I_{NOCT} = 800\ W/m^2$ (solar irradiance), and wind speed of 1 m/s. It is an empiric method developed to predict the PV cell temperature or more specifically the p-n junction temperature (Krauter & Priess, 2009). NOCT data such as $T_{NOCT}$ is provided by manufacturers and it is the standard method to predict PV cell temperature using only the ambient temperature and solar irradiance. There are international standards that are followed to find the NOCT depending on the PV technology. Manufacturers normally follow these standards. Alonso García & Balenzategui (2004) have applied these standards for different PV technologies and have assessed the accuracy of the predictions. They have found that

despite that NOCT not include wind cooling effects, the NOCT values varied within a ± 3°C range and that this variation only affected the yearly performance estimations within a ±1.5% range. The cell temperature $T_c$ is calculated using the following equation:

$$T_c = T_a + (T_{NOCT} - T_{a,NOCT}) \frac{I}{I_{NOCT}} \quad (2.1)$$

$T_a$ is the ambient temperature and $I$ is the in-plane irradiance. $T_{NOCT}$ is the nominal operating cell temperature at the standard test conditions of $T_{a,NOCT} = 20\,°C$, $I_{NOCT} = 800\,W/m^2$, and wind speed of 1 m/s. Typical $T_{NOCT}$ values can be found in **Table 2.1** for several commonly used PV technologies.

Table 2.1 Characteristics of commonly used PV technologies (Schwingshackl et al., 2013)

| **PV Technology** | **Monocrystalline silicon (m-Si)** | **Polycrystalline silicon (p-Si)** | **Amorphous silicon (a-Si)** | **Microcrystalline silicon (µc-Si)** | **Cadmium telluride (CdTe)** |
|---|---|---|---|---|---|
| Type | glass-polymer | glass-polymer | glass-glass | glass-polymer | glass-glass |
| $T_{NOCT}$ (°C) | 45 | 46 | 46 | 44 | 45 |
| $\eta_{STC}$ (%) | 18.4 | 14.1 | 6.0 | 9.5 | 10.7 |
| $\beta_{STC}$ (%/K) | -0.38 | -0.45 | -0.19 | -0.24 | -0.25 |
| $U_0$ | 30.02 | 30.02 | 25.73 | 30.02 | 23.37 |
| $U_1$ | 6.28 | 6.28 | 10.67 | 6.28 | 5.44 |

### 2.1.2 Sandia National Laboratory Methods

A PV cell temperature estimation model was developed by King et al. (2004) with Sandia National Laboratory (SNL) to improve the weak points of the NOCT model. This model includes parameters such as wind speed, type of PV encapsulation, and the configuration of the installations. It is a simple empirically based thermal model that was successful in predicting the PV cell temperature within an error range of ±5°C. This resulted in an error that is within ±3% in the energy generation prediction (King et al., 2004). The SNL model is presented in the following equation:

$$T_c = T_a + I.exp\ (a + bV_w) \quad (2.2)$$

$T_a$ is the ambient temperature, $I$ is the in-plane irradiance, and $V_w$ is the wind speed. The variables a and b are empirical coefficients that are obtained from **Table 2.2** according to module type and mounting configuration. These coefficients are determined empirically by using a module operating at near thermal equilibrium conditions. Thousands of temperature measurements over different days with different conditions have been recorded from the module to find these coefficients (King et al., 2004). At METU NCC, PV modules are of glass/cell/polymer sheet type and are open rack mounted therefore their corresponding values have been used where applicable from **Table 2.2**.

Table 2.2 Empirical coefficients of the SNL model for some typical types of PV module and its installation configurations (Trinuruk et al., 2009).

| **Module Type** | **Mount** | **a** | **b** | $\Delta T$ (℃) |
|---|---|---|---|---|
| Glass/cell/glass | Open rack | -3.47 | -0.0594 | 3 |
| Glass/cell/glass | Close roof mount | -2.98 | -0.0471 | 1 |
| Glass/cell/polymer sheet | Open rack | -3.56 | -0.0750 | 3 |
| Glass/cell/polymer sheet | Insulated back | -2.81 | -0.0455 | 0 |
| Polymer/thin film/steel | Open rack | -3.58 | -0.113 | 3 |

Another model was developed by King et al. (2004) to predict the PV cell temperature. It was used by Kurtz et al. (2009) to accurately predict the cell temperature using Typical Meteorological Year (TMY) data of several locations of different climatic conditions. It was reported that the model has predicted the monthly average module temperature within the accuracy of ±2°C. The model is presented in the following equation:

$$T_c = T_a + I.e^{-3.473-0.0594.V_w} \quad (2.3)$$

$T_a$ is the ambient temperature, $I$ is the in-plane irradiance, and $V_w$ is the wind speed. This relationship does not distinguish between different various PV technologies. It

was designed to predict PV cell temperatures of glass/cell/class modules that are rack-mounted (Kurtz et al., 2009).

### 2.1.3 Energy Balance Methods

In a study, Mattei et al. (2006) have developed a PV cell temperature estimation model based on a simple energy balance. The PV cell temperature was estimated using three models namely NOCT, energy balance method, and an optimized energy balance method. As the name implies, an energy balance for the module was used to formulate a relationship to estimate the PV cell temperature. Mattei proposed the following model for estimating PV cell temperature $T_c$ as follows:

$$T_c = \frac{U_{PV}(V_w)T_a + I.[\tau.\alpha - \eta_{STC}(1-\beta_{STC}T_{STC})]}{U_{PV}(V_w) + \beta_{STC}.\eta_{STC}.I} \quad (2.4)$$

$T_a$ is the ambient temperature, $I$ is the in-plane irradiance, and $V_w$ is the wind speed. $\beta_{STC}$ and $\eta_{STC}$ are the temperature coefficient of maximal power and efficiency respectively under standard test conditions (STC) which are: irradiance of 1000 $W/m^2$, $T_{STC} = 25$ ℃, and air mass $AM = 1.5$. The values of $\beta_{STC}$ and $\eta_{STC}$ can be found from **Table 2.1** according to the PV technology. $\tau$ is the transmittance of the cover system and $\alpha$ is the absorption coefficient of the cells. The value used by Mattei for $\tau.\alpha = 0.81$. As for $U_{PV}(V_w)$, it is the heat exchange coefficient for the total surface of the module, and it is found using the following equations for two different parameterizations used in the models suggested in Mattei 1 and Mattei 2 respectively:

$$U_{PV}(V_w) = 26.6 + 2.3V_w \quad (2.5)$$

$$U_{PV}(V_w) = 24.1 + 2.9V_w \quad (2.6)$$

An important thing to bear in mind here is that $\tau$ and $\alpha$ depend on the materials of the cover system and the cells, while $U_{PV}(V_w)$ depends on the wind direction and installation of the module. Although it is convenient to generally use the same values that Mattei used, it was shown that finding an optimized value for these variables

according to each case yielded more accurate results. The results with optimized $(\alpha\tau)$ coefficients yielded a root mean square error (RMSE) of 2.24°C while the results of using a generally specified correlation for $(\alpha\tau)$ has yielded an RMSE of 2.76 °C (Mattei et al., 2006). This indicates that in general optimizing PV cell temperature models for each case would yield more accurate results.

Another study by Bardhi et al. (2012) has compared different energy balance and thermal power exchange methods to predict the PV Cell Temperature. It was found that the radiative heat transfer component is not negligible and must be considered as it may lead to the underestimation or the overestimation of the PV cell temperature according to whether it is subjected to high solar radiation intensity or low solar radiation intensity respectively.

### 2.1.4 Simple Linear Model

An effective new approach by Muzathik (2014) was developed and used to to predict PV cell temperature. This model uses a simple formula to estimate the PV cell temperature using only solar irradiance, ambient temperature, and the wind speed. It was developed in Malaysia which has a tropical climate. Studies have shown that the suitability of many of the standard approaches such as NOCT are in question when considering tropical areas which have different environmental conditions compared to the specified conditions in NOCT. The accuracy of the NOCT model results are in question especially when the cooling of the module is poor (Muzathik, 2014). The PV Cell temperature can be found using the following relation:

$$T_c = 0.943T_a + 0.0195I - 1.528V_w + 0.3529 \quad (2.7)$$

$T_a$ is the ambient temperature, $I$ is the in-plane irradiance, and $V_w$ is the wind speed. The coefficients in **Equation 2.7** were developed empirically using simulations in MATLAB/Simulink using ambient temperature, solar irradiance, and wind speed data gathered over two years from 2008 to 2010. The cell temperature predictions of this model were found to have an error of ±3% when compared to measured data.

These results are satisfactory and means that this model can be used in areas with similar tropical climates. The suitability of this model in climatic conditions such as in Northern Cyprus is to be investigated.

### 2.1.5 Improved Wind Integrated NOCT Method

Skoplaki et al. (2008) have developed a simple semi-empirical correlation for estimating PV cell temperature. Wind data has been integrated to the standard NOCT model to improve its accuracy as NOCT does not consider the forced convection effect of wind on the PV cell temperature therefore affecting the cell temperature predictions. It is an advanced model that also integrates specific PV technology dependent properties such as the efficiency ($\eta$) and the temperature coefficient of maximal power ($\beta$) under standard test conditions (STC), in addition to the absorption coefficient of the cell ($\alpha$) and the transmittance of the encapsulation ($\tau$). These technology dependent properties can be obtained from **Table 2.1**. The following equation is the suggested by Skoplaki et al. (2008) to find the PV cell temperature:

$$T_c = T_a + \frac{I}{I_{NOCT}}\left(T_{NOCT} - T_{a,NOCT}\right).\frac{h_{w,NOCT}}{h_w(V)}.\left[1 - \frac{\eta_{STC}}{\tau.\alpha}(1 - \beta_{STC}T_{STC})\right] \quad (2.8)$$

$T_a$ is the ambient temperature, $I$ is the in-plane irradiance, and $V_w$ is the wind speed. $\beta_{STC}$, $\eta_{STC}$, and $T_{STC}$ are used as mentioned in **Section 2.1.3** Mattei. The value used by Skoplaki for $\tau.\alpha = 0.9$. As previously mentioned, it is more accurate to find and use the $\tau.\alpha$ of the PV module used. $h_w$ is the wind convection coefficient and is found using the following equations for two different parameterizations suggested by Skoplaki. In Eq. (8), $V_f$ is the wind speed measured 10 m above the ground whereas in Eq. (9) $V_w$ is the wind speed close to the PV module.

$$h_w(V_f) = 8.91 + 2.0V_f \quad (2.9)$$

$$h_w(V_w) = 5.7 + 2.8V_w \quad (2.10)$$

Skoplaki also found that the effect of free convection can be ignored for wind speeds above 1 m/s whereas it is significant to consider for wind speeds below 1 m/s. In the development of the suggested models, the free convection was ignored and therefore it is indicated to be used when the wind speed is greater than 1 m/s. The predicted cell temperature values were in the range of ±3°C from the measured cell temperature values for the studied wind speed range of 1-15 m/s which is considered a satisfactory result.

### 2.1.6 Simplified Hottel-Whillier-Bliss Method

A modified simpler version of the Hottel-Whillier-Bliss (HWB) equation was developed by Faiman (2008) to predict PV cell temperature with high accuracies. The HWB equation is used to determine the efficiency of a solar thermal collector and it was derived from an energy balance. It is simplified by neglecting the thermal heat exchange between the cell and the front/back sides resulting in a simpler heat exchange equation. The equation is presented as follows:

$$T_c = T_a + \frac{I}{U_0 + U_1 . V_w} \tag{2.11}$$

$T_a$ is the ambient temperature, $I$ is the in-plane irradiance, and $V_w$ is the wind speed. $U_0$ and $U_1$ are heat loss coefficients where $U_0$ here is a coefficient describing the radiation cooling effect on the module and $U_1$ is a coefficient that represents the cooling effect of the module by wind (Koehl et al., 2011). It is indicated and illustrated by Faiman (2008) that $U_0$ and $U_1$ should be experimentally found for each module type and location. Some module technology specific values for $U_0$ and $U_1$ were specified by Koehl et al. (2011) and can be found in **Table 2.1**. Faiman (2008) has concluded that the modified HWB equation yielded satisfactory PV cell temperature predictions within an accuracy of ±1.86K.

### 2.1.7 The $V_{OC}$-$I_{SC}$ Method

King et al. (2004) at Sandia National Laboratory have developed a model that uses electrical parameters to predict the PV cell temperatures. Such models do not use the ambient temperature, solar irradiance, and wind speeds to predict the cell temperature. Instead, electrical parameters are used to predict the cell temperature. The equation too predict the PV cell temperature is as follows:

$$T_c = (V_{oc} - V_{ocr} + \beta_{Voc}(X_c).T_r)/[n.k/q.\ln(I_{sc}/I_{scr}) + \beta_{Voc}(X_c)] \quad (2.12)$$

$T_c$ is the predicted PV cell temperature, $V_{oc}$ is the measured open-circuit voltage, and $I_{sc}$ is the measured short-circuit current. The solar cell parameters are $V_{ocr}$, $T_r$, and $I_{scr}$ at the reference point. $\beta_{Voc}$ is the open-circuit voltage temperature coefficient. *n*, *k*, and *q* are the cell ideality factor, the Boltzmann Constant, and the elementary charge respectively. $X_c$ is called the concentration ratio and it can be found using the following equation (King et al., 2004):

$$X_c = \frac{I_{sc}}{I_{scr}+\beta_{Iscr}.(T_c-T_r)} \quad (2.13)$$

An improved $V_{OC}$-$I_{SC}$ method was proposed by Ju et al. (2013) and was developed to predict the PV cell temperature of solar cells that are under concentrated solar radiation. The same parameters were used as in the original method with slight differences in the equation. The model is presented as follows:

$$T_c = [(V_{oc} - V_{ocr} - \frac{n.k.T_r}{q}.\ln(X_c)]/[\beta_{Vocr} + \frac{n.k}{q}.\ln(X_c)] + T_r \quad (2.14)$$

$T_c$ is the predicted PV cell temperature and $V_{oc}$ is the measured open-circuit voltage. The solar cell parameters are $V_{ocr}$, $T_r$, and $\beta_{Vocr}$ at the reference point. *n*, *k*, and *q* are the cell ideality factor, the Boltzmann Constant, and the elementary charge respectively. $X_c$ is the concentration ratio. The variables in this model are normally provided by manufacturers and therefore are easily obtained (Ju et al., 2013).

This model's results have been verified over a wide range of concentration ratios (for radiation) and cell temperatures. Its performance was compared to the standard $V_{OC}$-

$I_{SC}$ method over these ranges. As observed from **Figure 2.1**, both models perform similarly under lower concentration. As for at high concentrations, the improved method performs exceptionally well with an RMSE of 3.74°C while the standard method performs poorly.

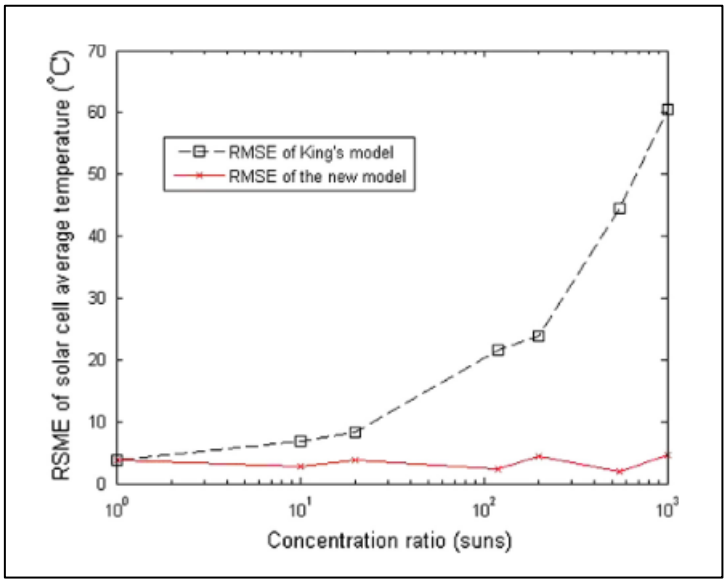


Figure 2.1 RMSE of the PV cell temperature predictions using the standard and improved $V_{OC}$-$I_{SC}$ methods (Ju et al., 2013)

### 2.1.8 Other Empirical Models in the Literature

The following section covers other empirical PV cell temperature estimation models that were developed in the literature. It is important to investigate whether a model performs well under each specific condition before using it for prediction. A model is more likely to perform better if the conditions (such as ambient temperature and solar irradiance) and the PV technology used match the specified conditions specified by the model. The following models are presented to shed the light on other methods in the literature for PV cell temperature predictions:

Ross (1976): $T_c = T_a + kI \; where \; k = \; \Delta\,(T_c - T_a)/\Delta I$ (2.15)

Rauschenbach (1980): $T_c = T_a + (I/I_{NOCT})/(T_{NOCT} - T_{a,NOCT})(1 - \frac{n_m}{\gamma_\alpha})$ (2.16)

Risser and Fuentes (1984): $T_c = 3.81 + 0.0282 \times I\ (1.31) \times T_a - 165V_w$ (2.17)

Schott (1985): $T_c = T_a + 0.028 \times I - 1$ (2.18)

Ross (1986): $T_c = T_a + 0.035 \times I$ (2.19)

Mondol et. al (2005, 2007): $T_c = T_a + 0.031I$ , $T_c = T_a + 0.031I - 0.058$ (2.20)

Lasnier and Ang (1990): $T_c = 30.006 + 0.0175(I - 300) + 1.14(T_a - 25)$ (2.21)

Servant (1985): $T_c = T_a + \alpha I(1 + \beta T\alpha)(1 - \gamma V_w)(1 - 1.053n_{m,ref})$ (2.22)

Duffle et al. (2006):

$$T_c = T_a + \left(\frac{I}{I_{NOCT}}\right)(9.5 - 5.7 \times 3.8V_w)(T_{NOCT} - T_{a,NOCT})(1-n_m) \quad (2.23)$$

A study conducted by Charles Lawrence et al. (2017) has proposed two new models to predict PV cell temperature but more specifically for floating PV technologies. During the study, the predictions of the before mentioned empirical methods for PV cell temperature estimations were compared to measured data and the results are presented in **Figure 2.2**. It is observed from the figure that the Lasnier and Ang model has performed best compared to the measured cell temperature. It is also noticed that as the solar irradiance increases the performance of all the models decline and the difference between predicted and measured cell temperatures are larger. Most of the models tend to overestimate the PV cell temperature at higher irradiance levels which consequently results in the underestimation of the energy generation.

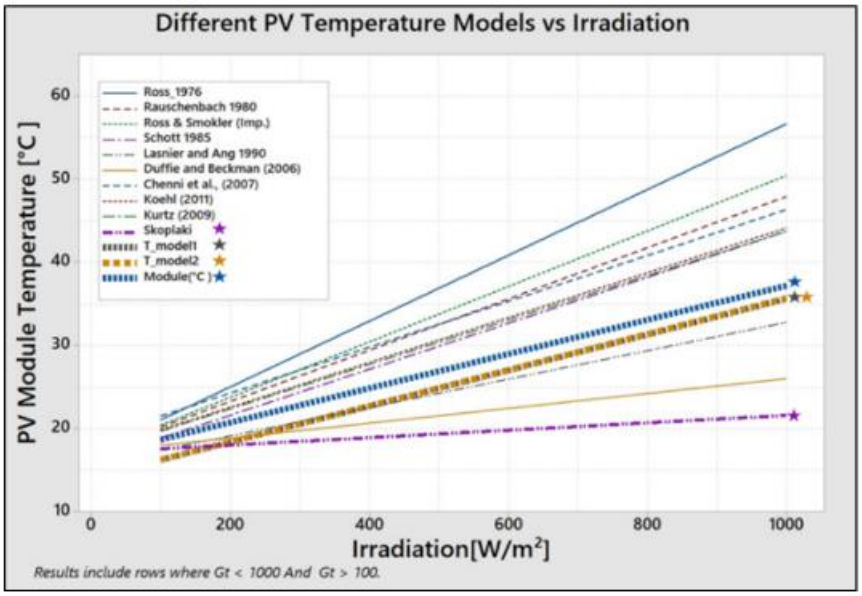


Figure 2.2 PV cell temperature prediction and PV cell temperature measurements versus solar irradiance (Charles Lawrence et al., 2017)

## 2.2 PV Cell Temperature Measurement Methods

One of the most important parameters for the precise evaluation of the performance of a PV module is the PV cell temperature. The last section was about the estimation of the PV cell temperature. This section focuses on the measurement techniques of the PV cell temperature that are mentioned in the literature. There are several techniques used in the literature with varying accuracies and costs. The choice of measurement technique depends on the required accuracy and the budget available.

Another important consideration is the variation between the PV cell temperature and the back temperature of a module. Some studies have measured the back temperature of a module and assumed that to be equal to the PV cell temperature whilst regarding the difference negligible. Other studies argued that the temperature difference between the module back side and the cell is significant and must be considered. Accordingly, they proposed one of two options the first being directly measuring the cell temperature which involves inserting the measuring device inside the module encapsulation and directly measuring the cell. This has disadvantages

which include the damaging of the module. The other option is to measure the back side temperature and use other proposed methods and relationships to relate it to the cell temperature. Results have shown that this is appropriate yields satisfyingly high accuracies.

### 2.2.1 PV Cell Temperature Measurement Using an Internal Thermocouple

In a study by Nishioka et al. (2018), the PV cell temperature was measured using a type-T thermocouple that was inserted inside the module encapsulation to directly measure the cell temperature rather than the back side temperature. In this case the thermocouple is in direct contact with the cell therefore it is expected to be a more accurate measurement. Practically, it is costly and hard to fabricate a specific module for this purpose therefore it may not be applicable on a large scale. This leads to the second part of the study which is to measure the backside temperature and compare it to the cell temperature found previously to investigate if it is appropriate to use the back side temperature as the cell temperature. **Figure 2.3** shows the setup used in the experiment.

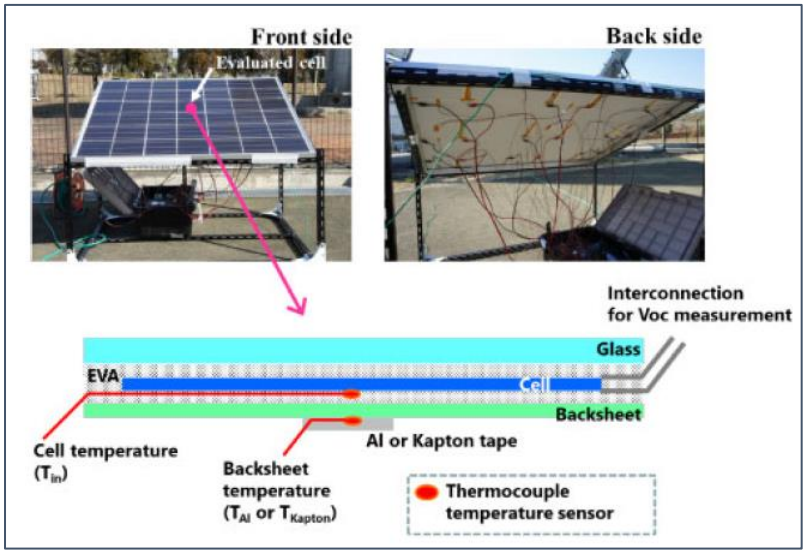


Figure 2.3 The setup of the fabricated module used to measure the PV cell temperature (Nishioka et al., 2018)

As observed from **Figure 2.3**, $T_{in}$ represents the cell temperature measurement by the thermocouple inserted inside the module while $T_{Al}$ represents the backside measurement by the thermocouples that were fixed to the back sheet with an aluminum tape. The results of this study have concluded that there is a significant difference between $T_{in}$ and $T_{Al}$ therefore it is not convincing to simply measure the backside and use it as the cell temperature (Nishioka et al., 2018). $T_{in}$ was found to be higher than $T_{Al}$ and this could be due to several reasons such as the different heat transfer properties of the back side and the cell as well as the convection effects of wind which is in direct contact with the back side.

Although it is possible to insert a thermocouple and measure $T_{in}$, it is not practical or easy to do so and it may damage the module. Alternatively, a temperature estimation model is proposed to use the irradiance and heat transfer properties of the materials of the module to find the cell temperature using the back side measurement. This method uses the heat flux diagram shown in **Figure 2.4** to estimate the cell temperature using the back side. In this figure, $T_4$ represents the cell temperature while $T_6$ represents the back side temperature measured by the thermocouple. The following heat transfer equation was used to find $T_4$ using $T_6$:

$$T_4 = T_6 + a\left(\frac{L_4}{\lambda_4} + \frac{L_5}{\lambda_5}\right) \times I \tag{2.24}$$

In the above equation, $a$ is a coefficient that is related to the heat retention property of the tape. It was found to be 0.22 and 0.49 for aluminum tape and klapton tape respectively. $L_4$ and $L_5$ are the thicknesses of the encapsulation and the backsheet as shown in **Figure 2.4**. $\lambda_4$ and $\lambda_5$ are the thermal conductivities of the encapsulation and the backsheet. $I$ is the solar irradiance. The results of the heatflux calculation showed that the predicted cell temperature $T_4$ was within ±1°C from the direct cell temperature measurement $T_{in}$ during the whole measurment duration. This shows that it is applicable to measure the module back temperature and use it to estimate the actual PV cell temperature with a high accuracy.

Another relationship was developed by King et al. (2004), that relates the cell temperature with the back side temperature. It is done assuming a one-dimensional heat conduction through the layers including the encapsulant and the back sheet. The relationship is presented as follows:

$$T_c = T_b + \frac{I}{I_o}.\Delta T \tag{2.25}$$

$T_c$ represents the cell temperature while $T_b$ represents the back side temperature measured by the thermocouple. $I$ is the solar irradiance and $I_o$ is the reference solar irradiance which is 1000 $W/m^2$. $\Delta T$ is the difference in temperature between the cell and the back side at 1000 $W/m^2$ irradiance level. It is indicated that $\Delta T$ is about 2-3°C for PV modules in an open rack mount. If the back side is thermally insulated then the difference between the back side and the cell temperature can be assumed to be zero (King et al., 2004).

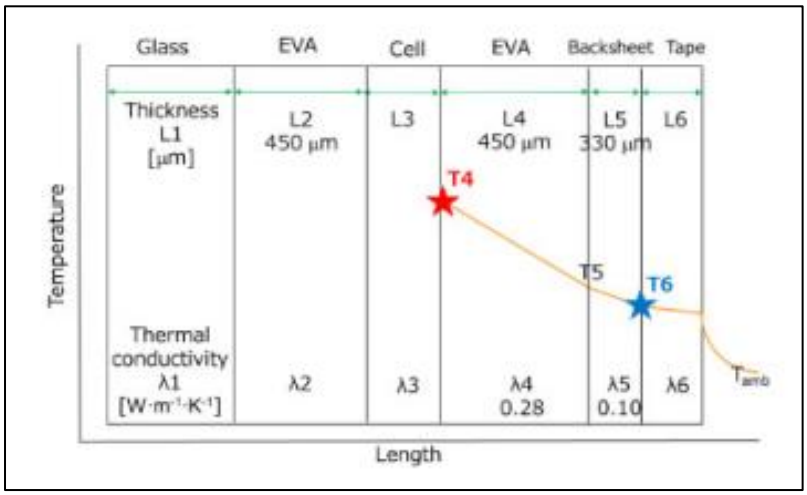


Figure 2.4 The PV module heat flux and structure (Nishioka et al., 2018)

### 2.2.2 PV Cell Temperature Measurement using RTDs and Thermocouples

Resistive Temperature Devices (RTD) are devices that use the change in resistance of the metal used to find the change in temperature. Thermocouples on the other hand

are thermoelectric sensors that sense the change in temperature through the change in voltage. The conventional method of PV cell temperature measurement is to install thermocouples and RTDs on the back side and average the readings to find the average PV cell temperature. Guay et al. (2016) has conducted a study that uses RTDs and thermocouples to measure the PV cell temperature and investigate whether the conventional method accurately represents the actual average temperature over the cells. The suitability of using a few RTDs on the back surface of a module and using it to measure the average cell temperature over a 1m length is investigated.

A total of 60 thermocouples and 10 RTDs were installed on the back of a 60-cell module. Each thermocouple was installed in the center of each cell while the RTDs were installed as close to the center as possible. **Figure 2.5** represents the setup of the instruments on the back side of the module.

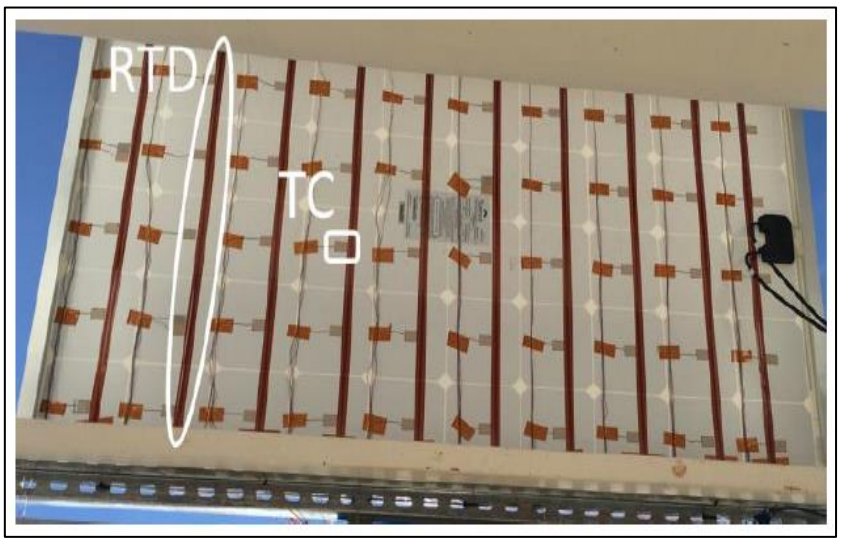


Figure 2.5 The setup of 60 thermocouples and 10 RTDs on the backside of the module (Guay et al., 2016)

The performance of each RTD was compared against the six corresponding thermocouples. After the experiment was carried out, it was found that the RTDs have consistently recorded the average of the six thermocouples as seen in **Figure 2.6**. This indicates that the RTDs are a good alternative for PV cell temperature

measurements. They provide accurate results with a smaller number of sensors. They are also easily installed and reused (Guay et al., 2016).

Another scope of the study was to investigate the conventional method of placing a few thermocouples at specific locations and averaging the readings to represent the average temperature across all the cells. A few measurements from four thermocouples at specific locations indicated by the standards of the IEC 61853 and Sandia National Laboratory were compared to the measurements of the 60 thermocouples. It was found that the IEC 61853 thermocouples have consistently underestimated the average cell temperature while the Sandia National Laboratory thermocouples have overestimated it (Guay et al., 2016). A thermal gradient map created from all 60 thermocouples has shown that the temperature of the module varies from cell to cell. It is then concluded that an adequate number of sensors must be used for accurate PV cell temperature measurements. This also depends on the measurement method and the type of sensor used as 6 RTDs were sufficient and have provided accurate measurements compared to the thermocouples.

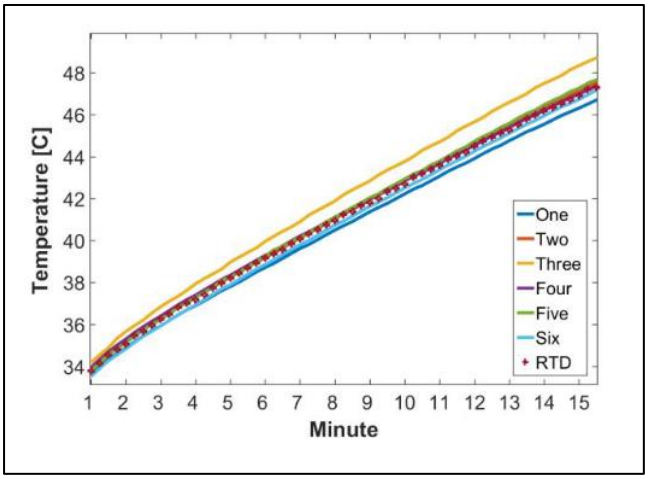


Figure 2.6 One RTD's temperature compared to the other six thermocouples (Guay et al., 2016)

### 2.2.3 PV Cell Temperature Measurement Using NTC Thermistors

The Negative Temperature Coefficient (NTC) Thermistor is a ceramic oxide semiconductor that can be used for high precision temperature measurement. It is inexpensive and accurate. A study by Mangeni et al., (2017) used NTC Thermistors to measure the PV cell temperature. Nine NTC thermistors were attached to the back of a PV module to find the cell temperature at nine corresponding locations. Using a heat distribution mapping technique, the temperature was found at a total of 81 points by linear interpolation.

The thermistors are connected to a microcontroller and a measurement circuit board as shown in **Figure 2.7**. The microcontroller digitizes the readings from the thermistors and then sends the data a computer. The NTC thermistors were attached to the back side of the module in a 3x3 manner as shown in **Figure 2.8**. They are all equally spaced. The thermistors were calibrated with, and its measurements were compared against a FLUKE infrared thermometer.

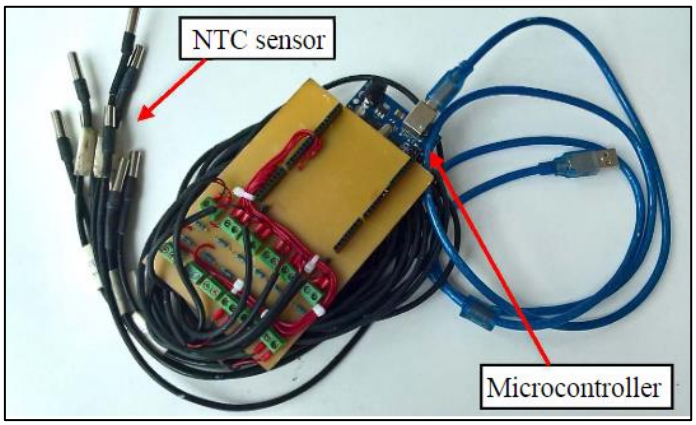


Figure 2.7 NTC sensor connected to an Arduino microcontroller (Mangeni et al., 2017)

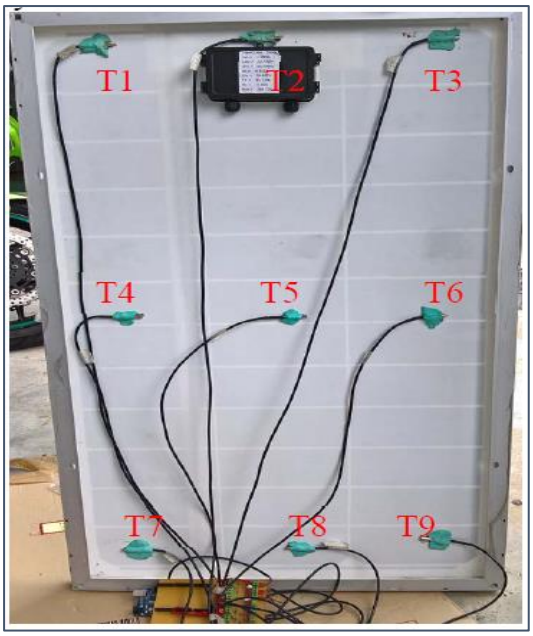


Figure 2.8 Nine NTC Thermistors attached to the back sheet of a module (Mangeni et al., 2017)

**Figure 2.9** shows the heat distribution map derived from the thermistors. The map was drawn for three different irradiance levels including 456 $W/m^2$, 581 $W/m^2$, and 642 $W/m^2$. It is observed that the heat distribution is generally non uniform at all irradiance levels but more specifically at lower irradiance levels. This again indicates that the more sensors used the more the measurements would be accurate.

**Figure 2.10** shows the heat distribution map of the 9 by 9 interpolated temperatures. As observed from the figure, having 81 mapping points results in a more uniform heat distribution across the map. The values at the 81 mapped points shown in **Figure 2.10** were compared to the measurements of the FLUKE infrared thermometer and an average error of $\pm 1°C$ was found. This concludes that the linear interpolation technique is applicable and provides satisfying results. This technique improves the accuracy of measurements and saves costs as higher precision results were achieved with less sensors (Mangeni et al., 2017). Additionally, NTC thermistors are considered inexpensive and an accurate temperature measurement device. Outstanding results were achieved using less sensors which are inexpensive in the first place making it an exceptional PV cell temperature measurement system.

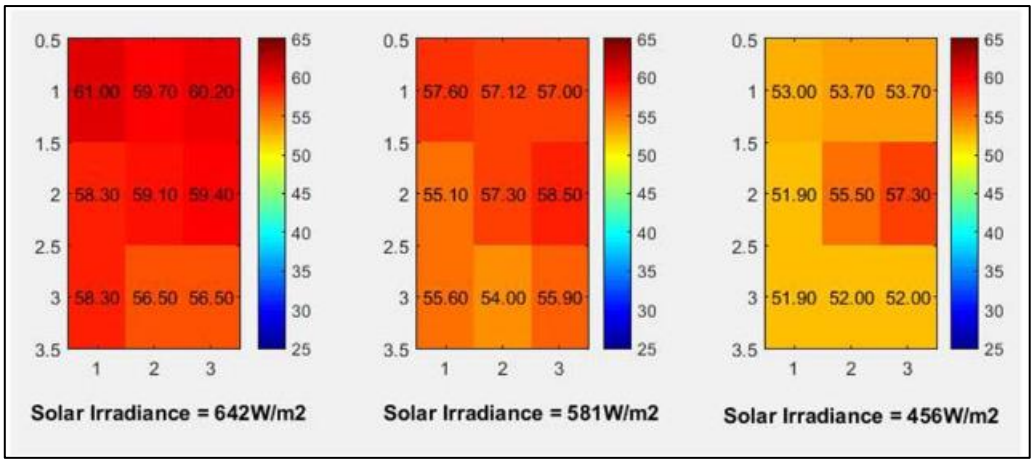


Figure 2.9 The heat distribution map of the module showing the temperature measured by the thermistors at different irradiance levels (Mangeni et al., 2017)

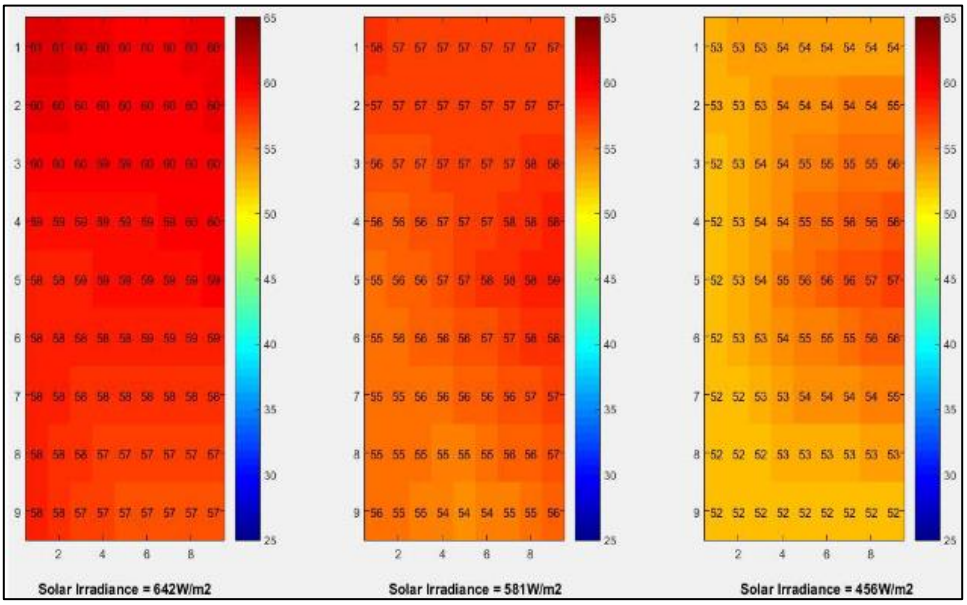


Figure 2.10 The heat distribution map of the 9 by 9 interpolated temperatures at different irradiance levels (Mangeni et al., 2017)

### 2.2.4 PV Cell Temperature Measurement Using Infrared System

Jovanović et al. (2017) have investigated the suitability of using a non-contact infrared system to accurately measure cell temperature. An IR sensor called MLX90614 (**Figure 2.11**) is connected to a microcontroller which is connected to a

computer is used to measure the PV cell temperature. A Jenoptik Varioscan thermal imaging camera was used to verify the results. The IR sensor comes factory calibrated so there is no need for calibration using this method.

In the setup, the IR sensor was placed 2 cm away from the module at a specific measurement spot. The sensor was placed perpendicular to the module. This is especially important when using IR sensors as the measurements are no longer accurate at angles of incidence above 30°C. The sensors were connected to PIC18F4550 microcontroller which was connected to a computer that records the date. The measurements took by the IR sensor were recorded for a several months during the duration of the study. It was found that the proposed IR sensor system has produced measurements that are in the range of ±0.5°C when compared to the measurements of the thermal imaging camera used for verification(Jovanović et al., 2017). This proves that it is a reliable system to be used for such applications.


Figure 2.11 MLX90614ESF-ACF Infrared Sensor (Jovanović et al., 2017)

This system is not only accurate and provides reliable results but has several other advantages that are important to highlight. Conventional systems that are used for temperature measurement usually involve contact sensors. Contact sensors may provide inaccurate results when the module is subjected to hot summer conditions where the solar radiation and the ambient temperature are high and the wind speed

is low. The module tends to heat up and the difference between the ambient temperature module temperature becomes very high up to 55°C (Jovanović et al., 2017). If the contact sensor is not well insulated, then the huge temperature difference will affect the accuracy of the measurements as the senor will be subject to the ambient temperature which is very different. The remedy for this problem is to thermally insulate the sensors properly but the IR sensor system eliminates the problem entirely.

Another advantage of the IR sensor system is its price. This system is inexpensive compared to many other measurement systems. For example, the price of a single Pt-100 RTD is around 50$ and the cost of a high precision system could range from 100$ to 500$. That is covering only the measurement of one module at a time. If the application requires the measurement of several modules, then the price significantly increases. On the other hand, the proposed system would cost about 30$ for the whole system which is one about one order of magnitude cheaper and produces very reliable results.

Jovanović et al. (2017) argues that for many applications, developing a low-cost system such as the one proposed or an NTC thermistor-based system is more convenient especially if the budget is an important consideration. These methods of PV cell temperature measurement can be very reliable if applied properly. He compared the proposed IR sensor system with a DS18B20 digital sensor system which is also connected to a microcontroller in the same manner discussed in this section. Both of these cell temperature measurement methods are within the same price range. Again, the measurements were verified using a thermal camera.

**Figure 2.12** shows the difference in cell temperature measurements between the proposed methods and the thermal imaging camera. The measurements of the IR sensor system were within ±0.5°C from the thermal imaging camera while the measurements of the digital sensor system were within ±1.5°C (Jovanović et al., 2017). This indicates that the IR sensor system is superior to the digital sensor system while both are within the same price range. The difference between the performance

of both systems could be due to the errors that arise when using a contact sensor. Regardless of the difference in performance of both the IR system and the digital sensor system, they have both proven to be reliable low-cost methods for PV cell temperature measurements.

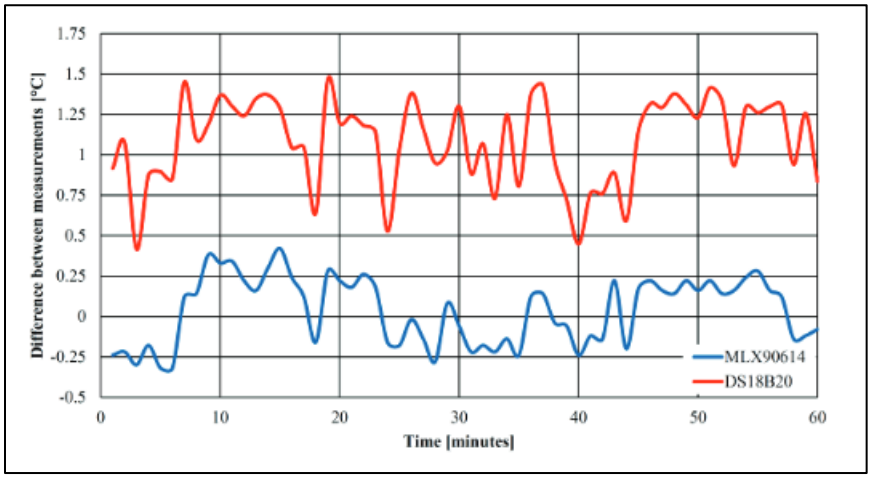


Figure 2.12 Graph showing the difference in measurements between the proposed systems and the thermal imaging camera (Jovanović et al., 2017)

## 2.3 The Effect of Soiling on the Performance of PV Modules

In general, large solar power plants are located in deserts and rural areas where abundant solar energy resources are available. This is also done to prevent buildings from attenuating and reflecting valuable solar resources away from the solar power plant. One important consideration especially in the above-mentioned locations of solar power plants is the high concentration of dust in the atmosphere which settles on PV modules and thus affecting its performance and causes the degradation of the modules. In this section, the effect of dust on the performance of PV modules is reviewed and discussed.

### 2.3.1 Environmental Factors that Affect the Soiling of PV Modules

Dust is present in the atmosphere with varying concentrations depending on the location and the surroundings. It is normally carried by wind from area to area and tends to settle and accumulate on surfaces over time. This procedure of the accumulation of dust on optical surfaces is called soiling. Soiling does not only occur due to the accumulation of dust. Other substances present in the atmosphere or the surroundings such as soil, salt, sand, organic materials, bird feces, ash, and many other substances may also cause the soiling of PV Modules.

The soiling effect on PV modules has been found in many studies to have a significant effect on the absorption of incident sun rays by PV modules and therefore causes power losses. Even though a desert or a rural area may have abundant solar resources, accumulated dust will affect the performance of PV modules considerably preventing the utilization of the solar resources. The main factor that influences the accumulation of dust is the location of the solar power plant. More specifically, the surrounding environment and its climatic conditions (Mani & Pillai, 2010). Environmental factors include the type of soil, type of terrain, and surrounding vegetation. Climatic factors include rain, wind speed, wind directions, dust storms, precipitation, humidity, and ambient temperature. **Figure 2.13** shows the daily output power losses due to soiling in different areas around the world. It is observed that the power losses in desert areas such as in Saudi Arabia is considerably greater than other areas that have Mediterranean climate such as in Cyprus or tropical climate such as in Nigeria. This is due to the difference in the environmental and climatic factors mentioned above.

The accumulation of dust in desert areas and areas that experience dust storms can be a challenge especially that dust storms are unpredictable and are not distributed over the year. The accumulation of dust in these arid areas that experience dust storms is considerably greater than other areas and therefore can affect the PV performance significantly. The ability to predict dust storms depends on the availability of meteorological data for the specific region. In some studies, dust

storms were predicted to be higher in specific months/seasons and accordingly required cleaning considerations were made (Dayan et al., 2008). This is important not only for the power losses but to prevent the degradation of PV modules in these harsh environments (Sayyah et al., 2014).

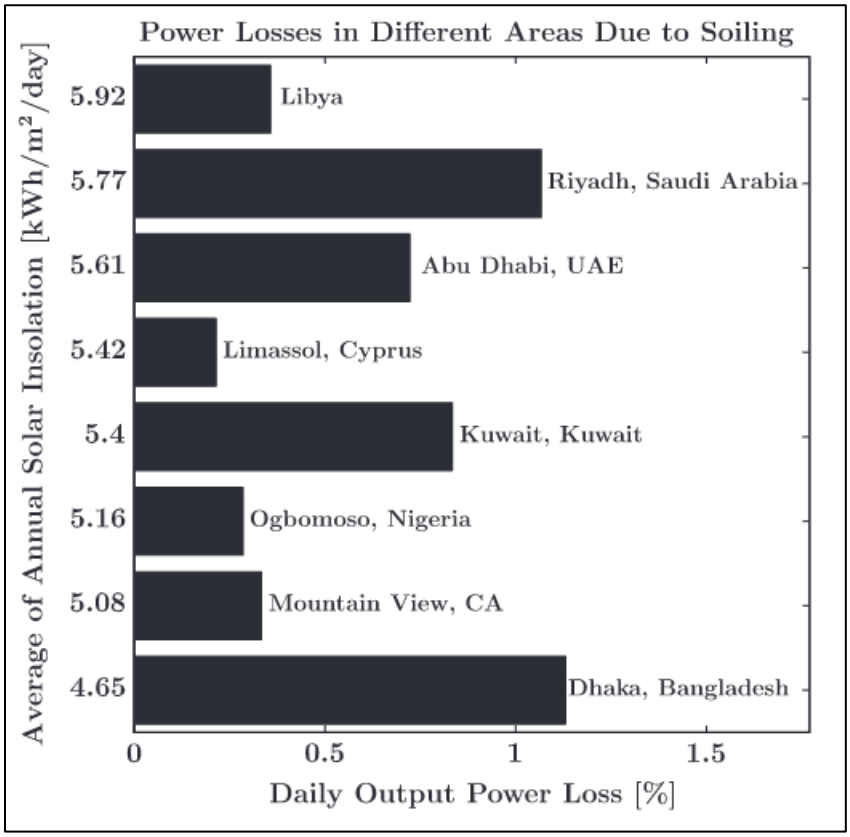


Figure 2.13 The daily output power losses in different areas with different environmental conditions (Sayyah et al., 2014)

Contrary to arid and desert areas that experience many dust storms and little to no rainfall, areas with excessive rainfall and surrounding vegetation experience less dust accumulation on PV Modules. These areas generally have less dust in the atmosphere. Rain also plays an important role in cleaning the accumulated dust from PV modules. For this reason, dust is seldom accumulated on PV modules that are in tropical areas and whenever it is, rainfall events clean the PV modules. On the other hand, areas that are dusty and rainy may sometimes experience dusty rain which

happens when rain collects the dust in the atmosphere and creates muddy patches on the surface of a PV panel (Haeberlin et al., 1998).

Another climatic condition that affects the accumulation of dust on PV modules is the wind. On one hand, it carries dust around and therefore can cause the accumulation of dust on the module. On the other hand, wind especially at high speeds removes deposited dust from PV modules. Whether wind will have a positive or negative effect on the accumulation of dust on PV modules depends on the wind speed, tilt angle, humidity, dust particle diameter, structure of the dust layer, and adhesion forces between the dust and the PV module (Hinds & Zhu, 1999). For example, if the weather is humid and dew is accumulated on the panel, then wind will cause the accumulation of dust as the dust carried by wind will stick to the panel.

Humidity is another climatic condition that affects the accumulation of dust on PV modules. In general humidity has a negative effect on the performance of PV modules as the high concentration of water vapor in the atmosphere absorbs solar radiation resulting in a decline in the solar irradiance. High relative humidity causes the formation of dew which causes the dust to stick to PV panel forming sticky layers that are hard to clean (Mekhilef et al., 2012). For this reason, desert areas close to huge water bodies may suffer from this problem immensely as atmospheric dust is abundant and the relative humidity is high. A study conducted by (Hoffman, 1980) has compared the accumulation of dust in a semi-arid location with a humid location in the USA. The study found out that the relative humidity is a very influential factor when considering dust deposition as it was significantly higher in the humid location.

Another problem that affects the performance of PV modules in some locations are bird droppings. While this may not be a problem in desert areas, other areas such as in offshore PV installations and areas with surrounding vegetation may experience this problem (Lamont & El Chaar, 2011). Bird droppings does not only affect the performance of PV modules but also its degradation. Bird feces is considered an organic material that when dropped on a module blocks incident sun rays and creates hot spots on the module that remain until cleaned. These hotspots cause the

degradation of the module over time. In addition to this, the metal frames of the module are subject to corrosion due to bird droppings (Appels et al., 2012).

A study was conducted to investigate the soiling effect on PV modules and compared the effect of dust deposition and the effect of bird droppings on three different PV installations. It was found that the effect of bird droppings has a significantly greater deteriorating effect on the performance of PV modules compared to dust deposition (Hammond et al., 1997). For this reason, it is important to remedy this problem effectively. Different methods such as non-toxic bird control products and low current barriers, bird nets, bird spikes, and even methods such as scaring birds with audibles were proposed (Ballinger Jr, 2001).

Other than the location of the solar power plant, there are several other factors that affect the power losses due to the accumulation of dust. The properties of accumulated dust such as dust particle size, dust type, composition of materials, charge distribution, and other biological properties also influence PV panel performance (Mani & Pillai, 2010). Although the properties of dust that is deposited on PV modules depend on the location and the environment, this will be discussed in another section.

### 2.3.2 Effect of the Tilt Angle on Soiling

The tilt angle of a PV panel has a significant effect on the amount of dust accumulation. For fixed tilt angle PV installations, the dust accumulation is the highest when the panel is horizontal at a 0° tilt angle. The dust accumulation decreases as the tilt angle decreases making it the least at a 90° tilt angle (Appels et al., 2012). This is because gravity is the main settling mechanism for dust. The greatest module surface area subject to dust settling due to gravity is when the tilt angle is 0° and facing upward. As the tilt angle increases, less module surface area is projected upwards. If the PV panel is vertical at a 90° angle, the diffusion of dust in the air becomes the main settling mechanism.

Normally, dust particles form adhesion forces due to dew from humidity or due to being electrostatically charged from the environment and thus sticking to the module. Dust particles with low adhesion forces tend to roll down the module's surface as the tilt angle increases. This rolling of dust of the module due to gravity cleans the module from dust. A similar concept applies to wind and rain. The cleaning of the modules by wind and rain depends on the tilt angle of the module with respect to the wind direction and rainfall direction (Hegazy, 2001).

A study was conducted Nahar & Gupta (1990) to study the effect of tilt angle on the accumulation of dust in an area that is subject to dust storms frequently. Three different PV modules were placed at a 0°, 45°, and 90° tilt angles. In a month with frequent dust storms, it was found that the modules with 0°, 45°, and 90° tilt angles have experienced a 6.28%, 4.62%, and 1.87% transmission loss due to dust accumulation respectively.

Another study by Elminir et al. (2006) was conducted to find the transmission loss of PV modules due to soiling for different tilt angles and orientations. From **Figure 2.14**, it is observed that the transmission losses have decreased consistently for all orientations as the tilt angle increased. At a 15° tilt angle, the transmission losses were about 20% and it decreased to about 5-8% at a 90° tilt angle for all orientations. This shows that regardless of which direction the PV is oriented, the tilt angle has a significant effect on the accumulation of dust on the module and correspondingly the attenuation of sunlight due to formed dust layers.

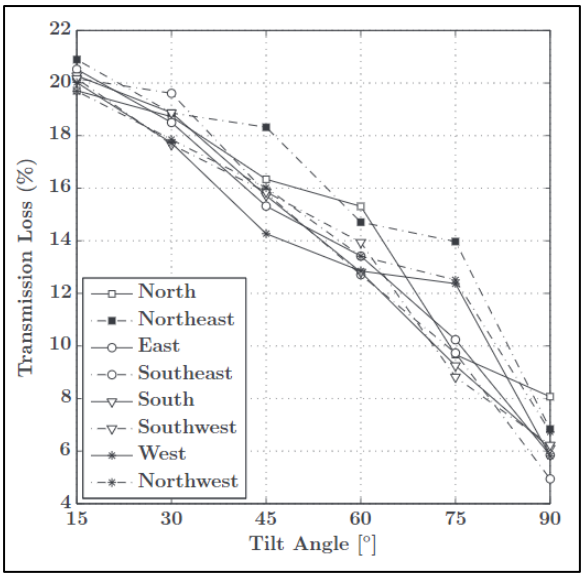


Figure 2.14 Transmission losses of PV modules for different tilt angles and orientations (Elminir et al., 2006)

Large scale PV systems are normally installed at a fixed tilt angle that is chosen according to the location so that the modules receive maximum possible solar radiation. Some PV systems are equipped with a solar tracking system that tracks sunlight to receive more solar radiation and thus generate more energy and output the maximum power possible. It was found that the solar tracking systems also influence the dust accumulation of PV modules.

Solar tracking systems can change the orientation of the module to minimize soiling, allow more convenient cleaning, and even face the modules down during dust storm events. In a study conducted by Cabanillas & Munguía (2011) PV modules equipped with a solar tracking system and fixed tilt angle modules have been exposed to sunlight in an outdoor environment for 20 days. The study has found that the modules with the solar tracking system have experienced less dust accumulation compared to the modules with a fixed tilt angle.

Another study by (Salim et al., 1988) has exposed three identical PV modules to an outdoor environment for a year. One module has a fixed tilt angle, one has a single axis solar tracking system, and the last one has a two-axis solar tracking system. The results have shown that the power output of the two-axis solar tracking system was

the highest followed by the single axis one and lastly the fixed tilt angle one. When the results were analyzed to find the reason, it was found that this was due to the higher rate of absorption of sunlight and due to less dust accumulation on the PV modules equipped with a solar tracking system.

### 2.3.3 Properties of Dust and Soiling Losses

The physical and chemical properties of dust have an affect the performance of PV modules. Several studies in the literature have investigated how different dust types of different particle sizes affect the attenuation of sunlight due to dust layers and the power output of PV modules. In a study by El-Shobokshy & Hussein (1993) different dust types including three types of limestone dust, cement, and carbon were accumulated on PV modules and were investigated to see their effect on the power output. Their particle diameters ranged from 5-80 μm. The results have shown that finer dust particles with smaller particle diameter have caused significantly greater power losses compared to coarser dust particles that have larger particle diameters at the same surface mass density of 25 $g/m^2$. This is because finer dust particles cause more scattering of sunlight due to having more specific surface area. The corresponding power and efficiency losses are shown in **Figure 2.15**. As observed from the figure, carbon has exhibited the largest losses as it has the finest dust particles of 5 μm diameter size.

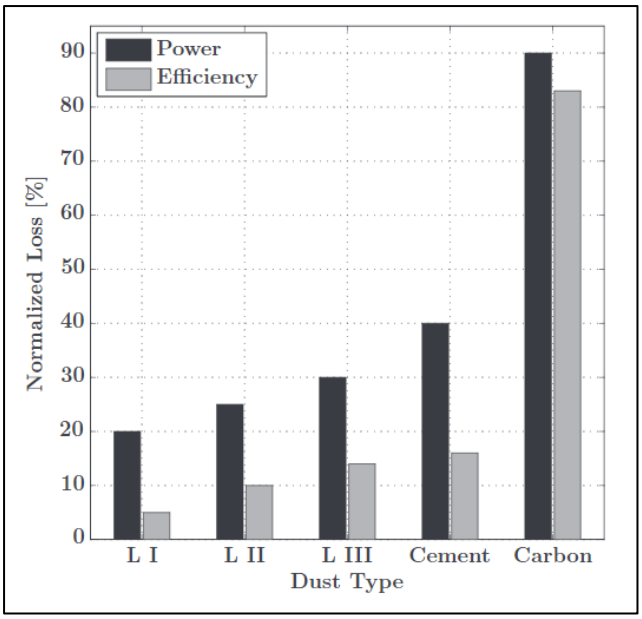


Figure 2.15 Power and efficiency losses for three different particle sizes of limestone, cement, and carbon at the surface mass density of 25 $g/m^2$ (El-Shobokshy & Hussein, 1993)

In another study, dust with particle diameters ranging from 10-75 µm was deposited on a PV module using a wind tunnel to investigate the effect of the particle size on the performance of PV modules. The results have shown that the particle diameter of dust has a significant effect on the mass density of the accumulation of dust and the attenuation of light caused by the dust layer. Dust of particle size of 30 µm has had 20% more deteriorating effect than dust of particle sizes of 75+ µm when the angle between the PV module and the direction of wind was 90° (Gaier & Perez-Davis, 1991). Again, this highlights the fact that dust with smaller particle size has a significantly larger deteriorating effect on the performance of PV modules when compared to dust of larger particle size.

Other than the physical properties such as the particle size, the chemical properties of different types of dust have an effect on the performance of PV modules. This highlights the importance of studying different dust types with different physical and chemical properties to see their varying effect on the performance of PV modules. Kaldellis et al. (2011) have studied the effect of the deposition of three different types

of dust namely ash, limestone, and red soil at different concentration densities on the performance of PV modules. The results are shown in **Figure 2.16**. When comparing the results of each dust type at similar concentration densities, it is observed that the deposition of red soil has had the most deteriorating effect on power loss followed by limestone then ash. This is more likely due to the different particle sizes and chemical properties of each dust type.

Sulaiman et al. (2011) have compared the effect of the deposition of mud and talcum powder on PV modules. Mud and talcum powder have been deposited with a dust layer thickness of 41 and 101 µm respectively. As observed from **Figure 2.17**, the power losses of mud are about 18% while talcum powder is about 16%. Although the power losses of both mud and talcum powder are similar, the dust layer thickness of the talcum powder deposited on the module is more than double of that of mud but has produced similar power losses. This similarity in power loss at different dust layer thickness is due to the physical and chemical properties of both dust types where mud demonstrated a more deteriorating effect at a lower thickness.

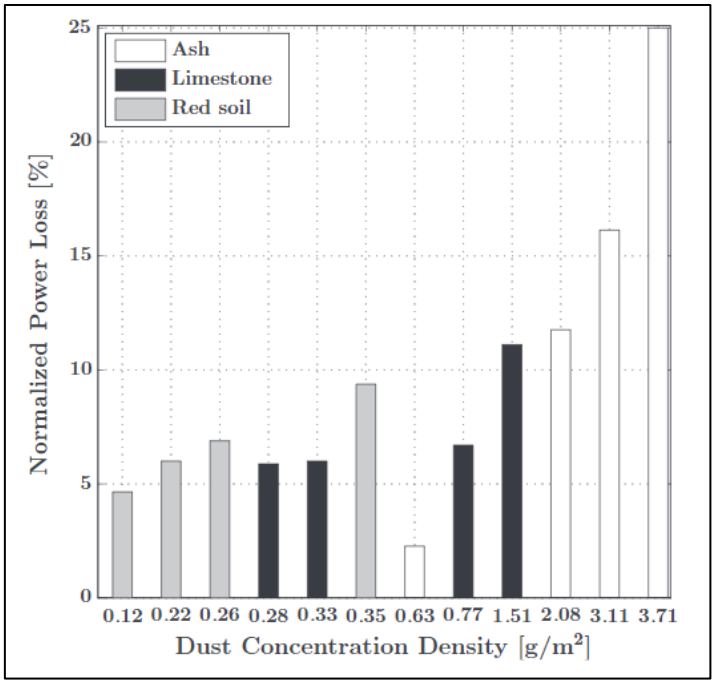


Figure 2.16 The power losses due to the deposition of ash, limestone, and red soil at different concentration densities on PV modules (Kaldellis et al., 2011)

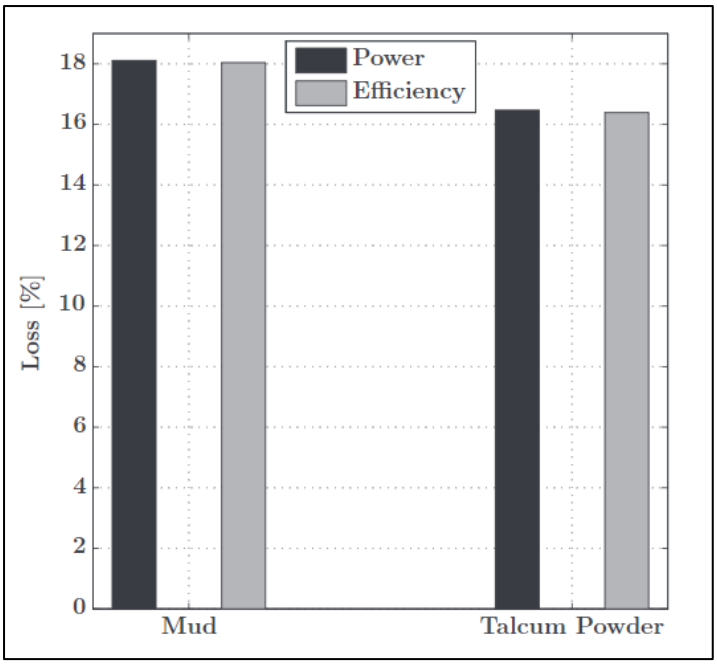


Figure 2.17 Power and efficiency losses due to deposition of mud and talcum powder on PV modules (Sulaiman et al., 2011)

To investigate the power losses due to dust deposition on the performance of PV modules by Molki (2010), up to 4 g of ground clay were deposited gradually on a 12 cm x 8 cm PV module. The power losses are illustrated in **Figure 2.18**. It is observed that the power losses increase as the mass of dust deposited increase. In addition, it is observed that as the concentration density of dust increases the rate of the output power loss decreases since the graph becomes less steep. This concludes that the highest rate of power loss occurs at lower dust concentration density and that at some point additional dust deposition has a less significant effect. In this case modules must be cleaned regularly as the highest rate of power loss occurs at lower dust concentration densities.

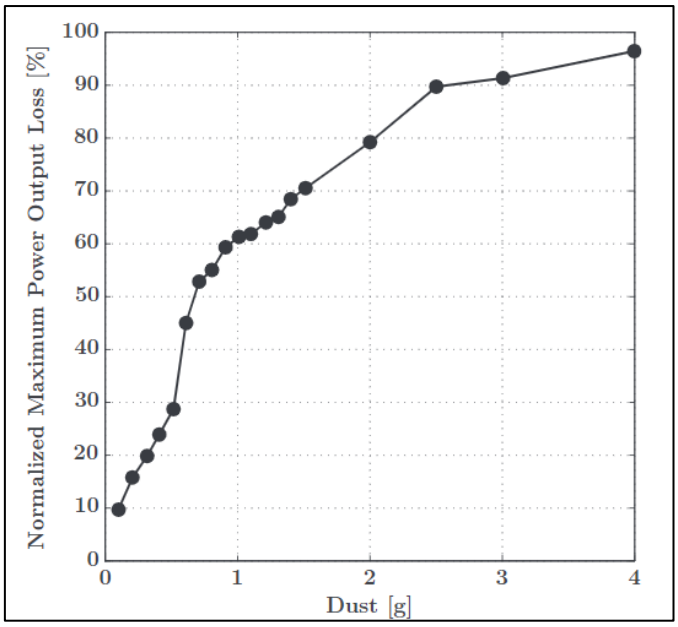


Figure 2.18 Power losses of up to 4 g of ground clay deposited on a 12 cm x 8 cm PV module (Molki, 2010)

# CHAPTER 3

# METHODOLOGY

In this chapter, the methodology and the experimental procedure done in this thesis is explained. This is divided into three sections which describe the procedure used for the PV cell temperature estimation, PV cell temperature measurement, and the soiling study conducted.

## 3.1 PV Cell Temperature Estimation

The PV cell temperature is a very important parameter used to assess the performance of PV modules on the short and long term. Accurate predictions of the cell temperature are necessary to be able to predict the energy production which is the main purpose of a solar power plant. The PV cell temperature is used to find the PV cell efficiency which determines how much of the incident solar radiation is turned into useful energy.

PV cell temperature estimation methods involve empirical equations developed by scientists over time to predict the PV cell temperature. These models are developed under specific testing conditions for a specific region or application. A PV cell temperature estimation model may or may not be suitable for some applications depending on the similarity of the conditions at hand with the conditions assumed during the development of the model. The most suitable PV cell temperature estimation models for Northern Cyprus summer conditions and more specifically for the METU NCC solar power plant are investigated.

Most PV cell temperature estimation models require the availability of the incident solar radiation, ambient temperature, and wind speed close to the module as inputs for the equations used for the prediction. These can be obtained using specific

measurement apparatus or in some locations may be obtained from a weather station or meteorological center. The solar radiation is measured using a pyranometer, the ambient temperature is measured using a thermometer or a wide range of sensors, and the wind speed is measured using an anemometer (shown in **Figures 3.1-3.3**). All the weather data was obtained from the METU NCC weather station.

Figure 3.1 Pyranometer

Figure 3.2 Thermometer

Figure 3.3 Anemometer

The solar radiation measurements obtained from the pyranometer represent the global solar radiation. In other words, this is the total solar radiation incident on earth and more specifically on a horizontal surface parallel to the ground. On the other hand, the solar radiation that is required for the prediction of the PV cell temperature is the incident or in-plane radiation which is the solar radiation received by the module according to its orientation. To do this a series of calculations must be done to find the angle of incidence which is used to find the in-plane radiation. These calculations involve geometric relations that are used to find out the direction of solar radiation at the location of the PV module. This depends on several factors including the time of the year, the position of earth with respect to the sun, the location on earth in question, etc. The following equations represent the calculations required to find the angle of incidence.

First, the declination angle ($\delta$) must be calculated. The declination angle is defined as the angular position of the sun at solar noon with respect to the equator. It is different for every day of the year. It is calculated using **Equation 3.1** where (*n)* is the day number out of 365 days per year.

$$\delta = 23.45°\sin[360°\left(\frac{284+n}{365}\right)] \quad (3.1)$$

The equation of time (*E)* is the difference between the time in terms of the position of the sun (solar time) and the time used in modern clocks. The equation of time is found using **Equation 3.2**. *B* is calculated using **Equation 3.3**.

$$E = 229.2[((7.5 * 10^{-5}) + 0.001868\cos(B) - 0.032033\sin(B) - 0.014615\cos(2B) - 0.04089\sin(2B))] \quad (3.2)$$

$$B = (n-1)\left(\frac{360°}{365}\right) \quad (3.3)$$

The solar time ($t_s$) is the time based on the position of the sun. It is found using **Equation 3.4** where ($t_{std}$) is the local time in decimals, ($L_{std}$) is the standard meridian for the local time zone in degrees, and ($L_{loc}$) is the longitude of the location in degrees.

$$t_s = t_{std} + \frac{4(L_{std} - L_{loc}) + E}{60} \quad (3.4)$$

There are two possible cases to consider when computing $L_{std}$. If the time zone of the location is positive, **Equation 3.5** is used. If the time zone is negative, then **Equation 3.6** is used.

$$L_{std} = 360° - TZ * 15° \quad (3.5)$$

$$L_{std} = -TZ * 15° \quad (3.6)$$

As for $L_{loc}$, if the longitude of the location is found in °W, then it is simply used as it is in **Equation 3.4**. If the longitude is in °E, then **Equation 3.7** is used.

$$L_{loc} = 360° - L_{loc} \quad (3.7)$$

The hour angle ($\omega$) is the solar time $t_s$ expressed as an angle and it is calculated using **Equation 3.8**.

$$\omega = (t_s - 12) * 15° \quad (3.8)$$

The zenith angle ($\theta_z$) is defined as the angle between vertical and beam radiation and it is found using **Equation 3.9** where ($\phi$) is the latitude of the location

$$cos\theta_z = cos\phi cos\delta cos\omega + \sin\phi sin\delta \quad (3.9)$$

The solar altitude angle ($\alpha_s$) is the complement if the zenith angle and it is found using **Equation 3.10**.

$$\alpha_s = 90° - \theta_z \quad (3.10)$$

The solar azimuth angle ($\gamma_s$) is the angle between south and the projection of beam radiation on a horizontal plane. To be able to calculate the azimuth angle, $\gamma_s'$ must be first calculated using **Equation 3.11** if $\theta_z \neq 0$. If $\theta_z = 0$, $\gamma_s' = 1$.

$$\gamma_s' = \frac{cos\theta_z * sin\emptyset - sin\delta}{sin\theta_z * cos\emptyset} \qquad if\ \theta z \neq 0 \quad (3.11)$$

If $\theta_z = 0$ and $\gamma_s' = 1$, $\gamma_s = 0$ and no further calculations are required. If $\gamma_s' \neq 1$, $\gamma_s$ is then calculated using **Equation 3.12** where ($sign\ (\omega)$) refers to the sign of the hour angle calculated previously. In other words, either (+) or (-).

$$\gamma_s = sign\ (\omega)\ |Acos(\gamma_s')| \qquad if\ \gamma_s' \neq 1 \quad (3.12)$$

The angle of incidence ($\theta$) is defined as the angle between beam radiation on a surface and the surface normal. Using the angle of incidence, the in-plane solar radiation can be found for the module. It is found using **Equation 3.13** where ($\beta$) is the tilt angle of the module.

$$cos\theta = cos\theta_z * cos\beta + sin\theta z * sin\beta * \cos(\gamma_s - \gamma) \quad (3.13)$$

The global (total) solar radiation has three main components which are beam, diffuse, and reflected radiation. Beam radiation ($I_b$) is the solar radiation received from the sun without being scattered by the atmosphere or any terrestrial objects. Diffuse radiation ($I_d$) is the solar radiation received from the sun after being scattered by the atmosphere such as by clouds. Reflected radiation ($I_\rho$) is the solar radiation received from the sun after being scattered or reflected by terrestrial objects. **Equation 3.14** represents all components of the global solar radiation. Measurements took by the pyranometer represent the global solar radiation ($I$) incident on a horizontal surface.

$$I = I_b + I_d + I_\rho \tag{3.14}$$

To find the beam radiation ($I_b$), **Equation 3.15** is used where ($I_{b,n}$) is the beam radiation parallel to the sun rays. It is also known as the direct normal insolation (DNI). $I_{b,n}$ can be measured using a pyrheliometer and then used to find $I_b$ which is essentially the vertical component of $I_{b,n}$ that is incident on a horizontal surface. The zenith angle ($\theta_z$) was used in this equation to find $I_b$ as it is the angle between vertical and beam.

$$I_b = I_{b,n} cos\theta_z \tag{3.15}$$

The pyranometer was used to measure $I$, and a pyrheliometer was used to measure $I_{b,n}$ and then used to calculate $I_b$. Since most large-scale PV installations are in non-urban areas, $I_\rho$ is normally neglected as there is no reflected radiation from buildings and other terrestrial objects. With that said, **Equation 3.14** is used to calculate $I_d$. The solar radiation values $I$, $I_b$, and $I_d$ represent the total solar radiation and its components that are incident on a horizontal surface. These values are now used to find the in-plane radiation that is incident on the tilted surface of the module.

The beam radiation incident on a tilted surface ($I_{b,t}$) is then found using **Equation 3.16**. Again, $I_{b,t}$ is the component of $I_{b,n}$ that is incident on a tilted surface. The angle of incidence found previously is used for this purpose as it is the angle between beam radiation and the tilted surface normal.

$$I_{b,t} = I_{b,n}\, cos\theta \tag{3.16}$$

The diffuse radiation incident on a tilted surface ($I_{d,t}$) is calculated using **Equation 3.17** where $I_d$ is the diffuse radiation incident on a horizontal surface and $\beta$ is the tilt angle of the module.

$$I_{d,t} = I_d \left(1 + \frac{cos\beta}{2}\right) \tag{3.17}$$

After finding $I_{b,t}$ and $I_{d,t}$, the total in-plane solar radiation incident on the module ($I_t$) can be found using **Equation 3.18**. This is done while assuming the reflected

component of solar radiation ($I_\rho$) to be zero as it was neglected as mentioned previously.

$$I_t = I_{b,t} + I_{d,t} \tag{3.18}$$

After finding the total in-plane solar radiation incident on the PV module ($I_t$), the ambient temperature, and the wind speed, the PV cell temperature is predicted using the PV cell temperature estimation models presented in **Equations 2.1-2.23**.

Furthermore, the PV cell efficiency ($\eta_{PV}$) is calculated using the PV cell temperature ($T_{cell}$) as shown in **Equation 3.19**. $\eta_{PV}$ represents the amount of the total in-plane incident solar radiation that is converted into output energy. The reference PV cell efficiency at standard test conditions ($\eta_{PV,ref}$) is the cell efficiency found by manufacturers while testing the module. The temperature coefficient ($\beta_{ref}$) is provided by the manufacturers which represents the variation in $\eta_{PV}$ as the cell temperature changes by 1°C. It has a value of 0.004 $k^{-1}$ for most silicon cells. The reference temperature ($T_{ref}$) is the ambient temperature specified by standard test conditions where $\beta_{ref}$ was found by the manufacturers.

$$\eta_{PV} = \eta_{PV,ref}\left[1 - \beta_{ref}\left(T_{cell} - T_{ref}\right)\right] \tag{3.19}$$

Finally, the energy generation of a single module ($I_{PV}$) is predicted using the PV cell efficiency by using **Equation 3.20**.

$$I_{PV} = (\eta_{PV})(I_t) \tag{3.20}$$

To find the total energy generation for a solar power plant ($E_{gen}$), **Equation 3.21** is used where $I_{PV}$ is the energy produced by a single module, *A* is the area of a single module, $\eta_{others}$ is the efficiency of the other components of the PV system, and the last term represents the number of modules. The term $\eta_{others}$ includes other efficiencies such as the inverter efficiency and cabling losses.

$$E_{gen} = I_{PV} * A * \eta_{others} * \left(\frac{PV\ plant\ capacity}{Module\ peak\ power}\right) \tag{3.21}$$

The predicted and the measured PV cell temperatures are used to find the PV cell efficiency and accordingly find the predicted and actual energy production. The accuracy of the cell temperature predictions is determined by comparing the results with actual PV cell temperature measurements. The root mean square error (RMSE) is used to compare a PV cell temperature estimation model's performance in estimating the PV cell temperature with the actual measured PV cell temperature and is shown in **Equation 3.22**. The procedure for measuring the PV cell temperature is explained in the next section.

$$RMSE = \sqrt{\frac{\sum_{i=1}^{n}(Predicted_i - Actual_i)^2}{n}} \tag{3.22}$$

To compare the predicted energy generation with the actual energy generation, the relative error (RE) is found and is calculated using **Equation 3.23.**

$$Relative\ Error = \frac{|Predicted\ Value - Actual\ Value|}{Actual\ Value} \times 100 \tag{3.23}$$

Microsoft Excel was used for the analysis of the data. An Excel model was designed to compute all the variables mentioned previously. The data is entered into the file and the necessary calculations are done. First, location, collector orientation, and PV specs data are entered into Microsoft Excel as shown in **Figure 3.4**. Then time, solar radiation, ambient temperature, and wind speed data are entered as shown in **Figure 3.5**. The data entered in **Figure 3.4** and **Figure 3.5**, are then used to calculate the solar geometry parameters required such as the zenith angle ($\theta_z$) and the angle of incidence ($\theta$) as shown in **Figure 3.6**.

Since the angle of incidence is now found, the in-plane solar radiation is now calculated and used to find the PV cell temperature as seen in **Figure 3.7**. Each of the PV cell temperature estimation models presented in **Equations 2.1-2.23** are used to predict the cell temperature. The models are formulated in the cells corresponding to the column $T_{cell}$ shown in **Figure 3.7**. Accordingly, the PV cell efficiency and the energy generation is calculated. The results of the predictions and measurements are compared using the RMSE and the RE as mentioned previously.

| | A | B | C | D | E | F | G | H | I | J |
|---|---|---|---|---|---|---|---|---|---|---|
| 1 | **Location:** | | | | | | | | **Solar Constant:** | |
| 2 | | | | Degrees | Minutes | | Direction | | $G_{sc}$ (W/m$^2$) | **1367** |
| 3 | Location: | **Guzelyurt** | Latitude: | **35** | **12** | | **N** | | | |
| 4 | Time Zone: | **2** | Longitude: | **33** | **1** | | **E** | | **PV Specs:** | |
| 5 | | | | | | | | | $\eta_{PV,ref}$ | **0.1500** |
| 6 | **Collector Orientation:** | | | | | | | | Area (m$^2$) | **0.34** |
| 7 | | | Degrees | | | | | | Peak Power (W) | **40** |
| 8 | Surface Azimuth (γ): | | **0** | | | | | | $G_{STC}$ (W/m$^2$) | **1000** |
| 9 | Surface Tilt (β): | | **30** | | | | | | $T_{STC}$ (°C) | **25** |
| 10 | | | | | | | | | NOCT (°C) | **45** |
| 11 | | | | | | | | | $G_{ref,\ NOCT}$ (W/m$^2$) | **800** |
| 12 | | | | | | | | | $T_{ref,\ NOCT}$ (°C) | **20** |
| 13 | | | | | | | | | $\beta_{ref}$ (1/K) | **0.0045** |

Figure 3.4 Excel model screenshot showing location, collector orientation, and PV specs data

| 15 | Time | | | Terrestrial Insolation | | Weather Conditions | |
|---|---|---|---|---|---|---|---|
| 16 | Month | Day | Hour | $I_{meas}$ | $I_{b,n\ meas}$ | $T_{amb}$ | $u_{W,meas,30m}$ |
| 17 | | | | ($Wh/m^2$) | ($Wh/m^2$) | ($^oC$) | (m/s) |
| 18 | 1 | 1 | 1 | 0 | 0 | 5.50 | 1.64 |
| 19 | 1 | 1 | 2 | 0 | 0 | 5.46 | 2.25 |
| 20 | 1 | 1 | 3 | 0 | 0 | 5.16 | 2.36 |
| 21 | 1 | 1 | 4 | 0 | 0 | 4.95 | 2.61 |
| 22 | 1 | 1 | 5 | 0 | 0 | 5.10 | 2.85 |
| 23 | 1 | 1 | 6 | 0 | 0 | 5.32 | 2.54 |
| 24 | 1 | 1 | 7 | 0 | 0 | 7.44 | 2.17 |
| 25 | 1 | 1 | 8 | 20 | 30 | 11.61 | 2.25 |
| 26 | 1 | 1 | 9 | 148 | 363 | 15.21 | 1.74 |
| 27 | 1 | 1 | 10 | 355 | 545 | 16.29 | 1.76 |
| 28 | 1 | 1 | 11 | 488 | 506 | 16.06 | 3.30 |
| 29 | 1 | 1 | 12 | 528 | 682 | 15.82 | 3.14 |
| 30 | 1 | 1 | 13 | 354 | 234 | 16.18 | 2.97 |
| 31 | 1 | 1 | 14 | 367 | 376 | 15.80 | 3.49 |
| 32 | 1 | 1 | 15 | 331 | 447 | 14.68 | 2.66 |
| 33 | 1 | 1 | 16 | 214 | 415 | 13.36 | 1.24 |
| 34 | 1 | 1 | 17 | 65 | 193 | 10.85 | 1.30 |
| 35 | 1 | 1 | 18 | 1 | 0 | 9.98 | 1.54 |

Figure 3.5 Excel model screenshot showing time, and weather-related data

| Solar Geometry Model | | | | | | | | | | | | | | | | | | | |
|---|---|---|---|---|---|---|---|---|---|---|---|---|---|---|---|---|---|---|---|
| Mid-hour | Day Number | Declination | | Equation of Time | | | Solar Time | Hour Angle | | Solar Zenith | | Solar Altitude | | Solar Azimuth | | | Angle of Incidence | | |
| | n | δ | | B | | E | $t_s$ | ω | | $\theta_z$ | | $\alpha_s$ | | $\gamma_s'$ | $\gamma_s$ | | θ | | cos(θ) |
| (hour) | | (rad) | (deg) | (rad) | (deg) | (min) | (hour) | (rad) | (deg) | (rad) | (deg) | (rad) | (deg) | (rad) | (rad) | (deg) | (rad) | (deg) | |
| 0.5 | 32 | -0.31 | -17.52 | 0.53 | 30.58 | -13.18 | 0.48 | -3.02 | -172.78 | 2.81 | 161.19 | -1.24 | -71.19 | -0.928344 | -2.76 | -158.18 | 2.81 | 161.19 | -0.95 |
| 1.5 | 32 | -0.31 | -17.52 | 0.53 | 30.58 | -13.18 | 1.48 | -2.75 | -157.78 | 2.68 | 153.49 | -1.11 | -63.49 | -0.5891 | -2.20 | -126.09 | 2.68 | 153.49 | -0.89 |
| 2.5 | 32 | -0.31 | -17.52 | 0.53 | 30.58 | -13.18 | 2.48 | -2.49 | -142.78 | 2.49 | 142.56 | -0.92 | -52.56 | -0.315486 | -1.89 | -108.39 | 2.49 | 142.56 | -0.79 |
| 3.5 | 32 | -0.31 | -17.52 | 0.53 | 30.58 | -13.18 | 3.48 | -2.23 | -127.78 | 2.28 | 130.61 | -0.71 | -40.61 | -0.11961 | -1.69 | -96.87 | 2.28 | 130.61 | -0.65 |
| 4.5 | 32 | -0.31 | -17.52 | 0.53 | 30.58 | -13.18 | 4.48 | -1.97 | -112.78 | 2.07 | 118.37 | -0.50 | -28.37 | 0.037641 | -1.53 | -87.84 | 2.07 | 118.37 | -0.48 |
| 5.5 | 32 | -0.31 | -17.52 | 0.53 | 30.58 | -13.18 | 5.48 | -1.71 | -97.78 | 1.85 | 106.20 | -0.28 | -16.20 | 0.178641 | -1.39 | -79.71 | 1.85 | 106.20 | -0.28 |
| 6.5 | 32 | -0.31 | -17.52 | 0.53 | 30.58 | -13.18 | 6.48 | -1.44 | -82.78 | 1.65 | 94.33 | -0.08 | -4.33 | 0.315952 | -1.25 | -71.58 | 1.65 | 94.33 | -0.08 |
| 7.5 | 32 | -0.31 | -17.52 | 0.53 | 30.58 | -13.18 | 7.48 | -1.18 | -67.78 | 1.45 | 83.04 | 0.12 | 6.96 | 0.457211 | -1.10 | -62.79 | 1.45 | 83.04 | 0.12 |
| 8.5 | 32 | -0.31 | -17.52 | 0.53 | 30.58 | -13.18 | 8.48 | -0.92 | -52.78 | 1.27 | 72.67 | 0.30 | 17.33 | 0.605971 | -0.92 | -52.70 | 1.27 | 72.67 | 0.30 |
| 9.5 | 32 | -0.31 | -17.52 | 0.53 | 30.58 | -13.18 | 9.48 | -0.66 | -37.78 | 1.11 | 63.74 | 0.46 | 26.26 | 0.758717 | -0.71 | -40.65 | 1.11 | 63.74 | 0.44 |
| 10.5 | 32 | -0.31 | -17.52 | 0.53 | 30.58 | -13.18 | 10.48 | -0.40 | -22.78 | 0.99 | 56.98 | 0.58 | 33.02 | 0.897825 | -0.46 | -26.13 | 0.99 | 56.98 | 0.54 |
| 11.5 | 32 | -0.31 | -17.52 | 0.53 | 30.58 | -13.18 | 11.48 | -0.14 | -7.78 | 0.93 | 53.23 | 0.64 | 36.77 | 0.986936 | -0.16 | -9.27 | 0.93 | 53.23 | 0.60 |
| 12.5 | 32 | -0.31 | -17.52 | 0.53 | 30.58 | -13.18 | 12.48 | 0.13 | 7.22 | 0.93 | 53.16 | 0.64 | 36.84 | 0.988717 | 0.15 | 8.62 | 0.93 | 53.16 | 0.60 |
| 13.5 | 32 | -0.31 | -17.52 | 0.53 | 30.58 | -13.18 | 13.48 | 0.39 | 22.22 | 0.99 | 56.78 | 0.58 | 33.22 | 0.902294 | 0.45 | 25.54 | 0.99 | 56.78 | 0.55 |
| 14.5 | 32 | -0.31 | -17.52 | 0.53 | 30.58 | -13.18 | 14.48 | 0.65 | 37.22 | 1.11 | 63.45 | 0.46 | 26.55 | 0.764289 | 0.70 | 40.16 | 1.11 | 63.45 | 0.45 |
| 15.5 | 32 | -0.31 | -17.52 | 0.53 | 30.58 | -13.18 | 15.48 | 0.91 | 52.22 | 1.26 | 72.31 | 0.31 | 17.69 | 0.611619 | 0.91 | 52.29 | 1.26 | 72.31 | 0.30 |
| 16.5 | 32 | -0.31 | -17.52 | 0.53 | 30.58 | -13.18 | 16.48 | 1.17 | 67.22 | 1.44 | 82.63 | 0.13 | 7.37 | 0.462587 | 1.09 | 62.45 | 1.44 | 82.63 | 0.13 |
| 17.5 | 32 | -0.31 | -17.52 | 0.53 | 30.58 | -13.18 | 17.48 | 1.44 | 82.22 | 1.64 | 93.90 | -0.07 | -3.90 | 0.321084 | 1.24 | 71.27 | 1.64 | 93.90 | -0.07 |
| 18.5 | 32 | -0.31 | -17.52 | 0.53 | 30.58 | -13.18 | 18.48 | 1.70 | 97.22 | 1.85 | 105.75 | -0.27 | -15.75 | 0.183739 | 1.39 | 79.41 | 1.85 | 105.75 | -0.27 |
| 19.5 | 32 | -0.31 | -17.52 | 0.53 | 30.58 | -13.18 | 19.48 | 1.96 | 112.22 | 2.06 | 117.92 | -0.49 | -27.92 | 0.043061 | 1.53 | 87.53 | 2.06 | 117.92 | -0.47 |
| 20.5 | 32 | -0.31 | -17.52 | 0.53 | 30.58 | -13.18 | 20.48 | 2.22 | 127.22 | 2.27 | 130.16 | -0.70 | -40.16 | -0.113272 | 1.68 | 96.50 | 2.27 | 130.16 | -0.64 |
| 21.5 | 32 | -0.31 | -17.52 | 0.53 | 30.58 | -13.18 | 21.48 | 2.48 | 142.22 | 2.48 | 142.13 | -0.91 | -52.13 | -0.307126 | 1.88 | 107.89 | 2.48 | 142.13 | -0.79 |

Figure 3.6 Excel model screenshot of the solar geometry model

| Solar Resource Model | | | | | | | PV Energy Model | | | |
|---|---|---|---|---|---|---|---|---|---|---|
| Terrestrial | | | | Terrestrial Tilted | | | | | for single module | for plant |
| I (Wh/m²) | $I_d$ (Wh/m²) | $I_b$ (Wh/m²) | $I_{b,n}$ (Wh/m²) | $I_t$ (Wh/m²) | $I_{d,t}$ (Wh/m²) | $I_{b,t}$ (Wh/m²) | $T_{cell}$ (°C) | $\eta_{PV}$ (%) | $I_{PV}$ (Wh/m²) | $E_{gen}$ (kWh) |
| 0 | 0 | 0 | 0 | 0 | 0 | 0 | 11.8 | 16.22211 | 0 | 0 |
| 0 | 0 | 0 | 0 | 0 | 0 | 0 | 11.25 | 16.25762 | 0 | 0 |
| 0 | 0 | 0 | 0 | 0 | 0 | 0 | 10.7 | 16.29312 | 0 | 0 |
| 0 | 0 | 0 | 0 | 0 | 0 | 0 | 10.25 | 16.32217 | 0 | 0 |
| 0 | 0 | 0 | 0 | 0 | 0 | 0 | 9.95 | 16.34154 | 0 | 0 |
| 0 | 0 | 0 | 0 | 0 | 0 | 0 | 9.7 | 16.35768 | 0 | 0 |
| 0 | 0 | 0 | 0 | 0 | 0 | 0 | 9.6 | 16.36413 | 0 | 0 |
| 61 | 45.24207 | 15.75793 | 130 | 61 | 45.24207 | 15.75793 | 11.90625 | 16.21525 | 9.891305 | 64.36786 |
| 148 | 125.6591 | 22.3409 | 75 | 148 | 125.6591 | 22.3409 | 15.525 | 15.98165 | 23.65284 | 153.9213 |
| 223 | 200.879 | 22.12096 | 50 | 223 | 200.879 | 22.12096 | 18.86875 | 15.7658 | 35.15773 | 228.7896 |
| 299 | 262.4859 | 36.51408 | 67 | 299 | 262.4859 | 36.51408 | 22.24375 | 15.54793 | 46.4883 | 302.5236 |
| 383 | 291.4157 | 91.58426 | 153 | 383 | 291.4157 | 91.58426 | 25.91875 | 15.31069 | 58.63995 | 381.6006 |
| 388 | 291.468 | 96.53195 | 161 | 388 | 291.468 | 96.53195 | 26.975 | 15.24251 | 59.14092 | 384.8607 |
| 369 | 290.1051 | 78.89489 | 144 | 369 | 290.1051 | 78.89489 | 26.98125 | 15.2421 | 56.24336 | 366.0048 |
| 297 | 208.9362 | 88.0638 | 197 | 297 | 208.9362 | 88.0638 | 25.08125 | 15.36475 | 45.63332 | 296.9598 |
| 243 | 93.18703 | 149.813 | 493 | 243 | 93.18703 | 149.813 | 23.49375 | 15.46723 | 37.58538 | 244.5876 |
| 104 | 53.7441 | 50.2559 | 392 | 104 | 53.7441 | 50.2559 | 18.85 | 15.76701 | 16.39769 | 106.7083 |
| 1 | 1 | 0 | 0 | 1 | 1 | 0 | 14.88125 | 16.02321 | 0.160232 | 1.042713 |
| 0 | 0 | 0 | 0 | 0 | 0 | 0 | 14.1 | 16.07364 | 0 | 0 |
| 0 | 0 | 0 | 0 | 0 | 0 | 0 | 13.45 | 16.1156 | 0 | 0 |
| 0 | 0 | 0 | 0 | 0 | 0 | 0 | 12.95 | 16.14788 | 0 | 0 |

Figure 3.7 Excel model screenshot showing the solar resource model and the PV energy model

## 3.2 PV Cell Temperature Measurement

The estimation of the PV cell temperature and the energy generation has been discussed in the previous section. In this section, the measurement of the PV cell temperature is discussed. The predictions obtained and the actual PV cell temperature must be compared to assess the accuracy of the prediction models. Several PV cell measurement methods are available in the literature, and each have their unique advantages and disadvantages. In this thesis, PV cell measurement using negative temperature coefficient (NTC) thermistors is chosen as it is the most convenient and practical method yielding satisfactory results.

Several studies in the literature have proposed the use of NTC thermistors for measuring the PV cell temperature. NTC thermistors are considered inexpensive and are an accurate temperature measurement device. Outstanding temperature

measurement results have been achieved using a smaller number of sensors which are cost-effective making it an exceptional PV cell temperature measurement method.

NTC thermistors are high precision ceramic oxide semiconductors that are used for many applications that involve temperature measurements. As the temperature of the thermistor increases, the resistance decreases and vice versa. The change in resistance is measured and accordingly the corresponding temperature is found. For the purpose of measuring the PV cell temperature, a 10-k NTC thermistor was used which has a 1% precision value. 10-k thermistors are named in this manner because they have 10 kΩ resistance at $25\ °C$. This is how thermistors are generally specified. Its operating range for temperature measurement is between -55°C to 125°C. **Equation 3.24** relates the temperature and the resistance of the thermistor, and it is used to find the temperature sensed by the thermistor using the resistance.

$$T = \frac{1}{((\frac{1}{B_o})(\log\frac{R}{R_o})) + (\frac{1}{T_o})} - 273.15 \tag{3.24}$$

$T_o$ is the nominal temperature, $B_o$ is the nominal beta constant at $T_o$, $R_o$ is the nominal resistance at $T_o$, and $R$ is the resistance. For the thermistor used in this thesis, $T_o = 25\ °C = 298.15\ K$, $B_o = 3950$, and $R_o = 10\ k\Omega$. All nominal data is provided by the manufacturers.

The resistance of the thermistor ($R$) is found by constructing a voltage divider circuit where the 10-k thermistor is connected in series with a 10-k resistor. A 5V power supply is used to power the circuit and it is supplied by the microcontroller used. The resistor and the thermistor are connected to the analog pin of the microcontroller which reads the voltage across the thermistor and converts it into digital form that can then be processed by the microcontroller. This is shown in **Equation 3.25**.

$$ADC = V_{out} * \left(\frac{1024}{V_{ref}}\right) \tag{3.25}$$

The measured resistance of the thermistor ($R$) is then calculated using **Equation 3.26** and is used in **Equation 3.24** to find the temperature.

$$R = \frac{R_o}{\left(\frac{1024}{ADC}\right) - 1} \tag{3.26}$$

An Arduino Mega microcontroller was programmed using **Equations 3.24-3.26** to find the resistance of the NTC thermistor and accordingly calculate the temperature. Nine NTC thermistors were used to measure the PV cell temperature of the back of the module. Arduino Mega was chosen as it offers 16 analog pins compared to Arduino Uno which has only 6. The voltage divider circuit was constructed using the thermistors, resistors and the Arduino Mega. The Arduino is then connected to a notebook computer where a code on the Arduino application was created to find and display the temperature of each sensor. The code is available in **Appendix A**.

To be able verify the temperature measurements of the thermistors and check if calibration is needed, the resistance value of the thermistor was checked at different temperatures. If the resistance of the thermistor at different temperatures matched the resistances in the thermistor output table provided by the manufacturers, then no calibration is needed. The temperature found by the thermistor was verified using a thermometer. The thermistor output table is provided in **Appendix B**.

A PV cell temperature measurement system was created using nine thermistor sensors attached to the back of a monocrystalline silicon technology PV module. The components that were used to create the NTC thermistor-based PV cell temperature measurement system used in this study are presented as follows:

- Monocrystalline silicon PV module (**Figure 3.8**)
- Nine 10-k NTC thermistors (**Figure 3.9**)
- Wires
- Soldering board (**Figure 3.10**)
- Nine 10 $k\Omega$ resistors (**Figure 3.10**)
- Arduino Mega microcontroller (**Figure 3.10**)

- USB cable
- Notebook computer
- Silicon heat transfer compound (**Figure 3.11**)
- Glue pad (**Figure 3.11**)
- Thermal insulation tape (**Figure 3.11**)
- Solar panel adjustable base (**Figure 3.13**)

First, the PV module shown in **Figure 3.8** was cleaned from the front and back side to remove any dust particles. Nine of the thermistors shown in **Figure 3.9** were soldered to long wires to be able to extend them from the back side of the module to the soldering board where the voltage divider circuit is created. The thermistors and the resistors are then soldered to the soldering board and the voltage divider circuit is created and connected to the Arduino Mega microcontroller as show in **Figure 3.10**.

Figure 3.8 Monocrystalline silicon PV module

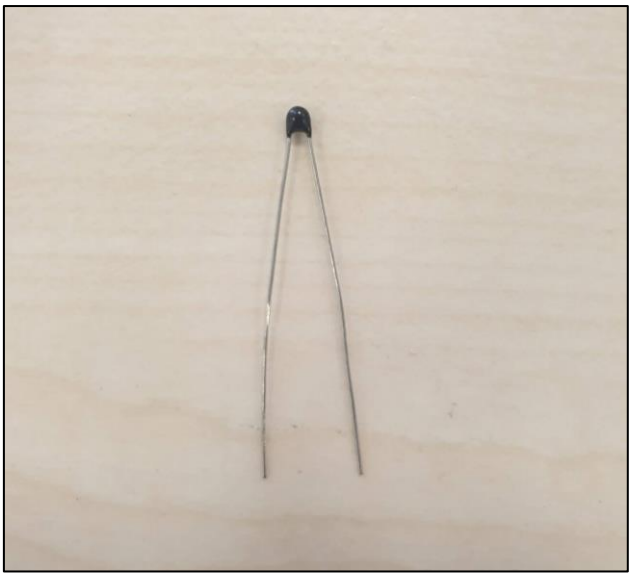

Figure 3.9 10-k NTC Thermistor

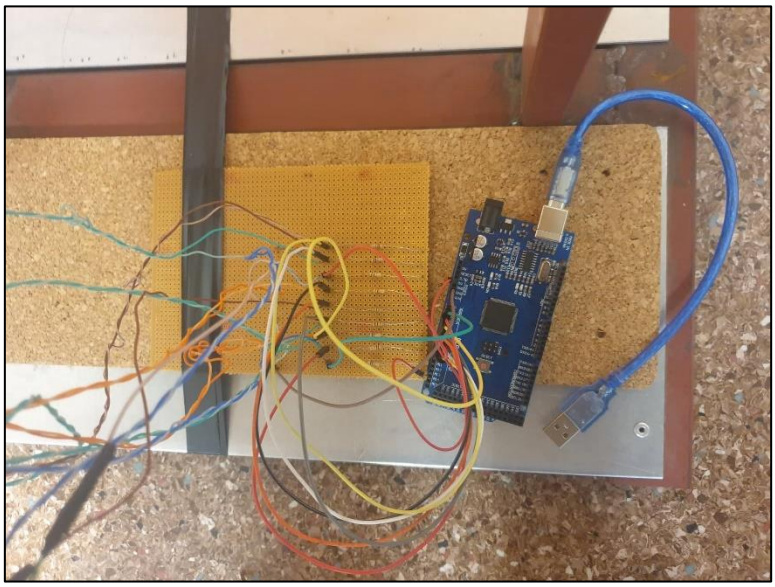

Figure 3.10 Voltage divider circuit including thermistors, resistors, and Arduino Mega microcontroller

After creating the voltage divider circuit on the soldering board for all nine thermistors that are used as temperature sensors for measuring the PV cell temperature, the thermistors are then attached to the back side of the PV module.

Glue pads, thermal insulation tape, and silicon heat transfer compound are used for this process and are shown in **Figure 3.11.**


Figure 3.11 Silicon heat transfer compound, thermal insulation tape, and glue pads

First, silicon heat transfer compound is applied to the thermistors to maximize the contact surface area between the thermistors and the back side surface of the module. The thermistors are then attached to the back side of the module using glue pads at nine different equidistant locations to find the average cell temperature of the module. Finally, a thermal insulating tape was used to cover all the thermistors to ensure thermal insulation between them and the surroundings so that the PV cell temperature measurements are not affected by the ambient temperature. The back side of the module after all the thermistors were attached is shown in **Figure 3.12**.

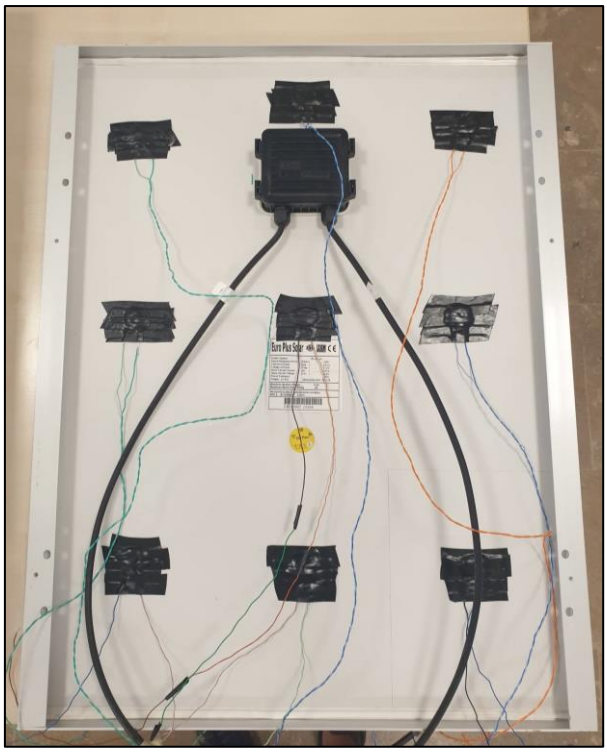

Figure 3.12 Back side of PV module after nine NTC thermistors are attached

Finally, the PV module is then attached to the PV module adjustable base shown in **Figure 3.13**. The tilt angle (β) used for the module is 30° as it is in the METU NCC power plant to mimic the power plant installation and keep the factors the same to generalize the results for the METU NCC solar power plant.

The setup is now ready for PV cell temperature measurement. The PV module is placed outdoors in a location close to the METU NCC power plant and in a similar orientation. The PV module was exposed to the sunlight for 15-30 mins to reach thermal equilibrium before any data is recorded. A USB cable is used to connect the Arduino microcontroller to a notebook computer. The Arduino software is opened on the computer, the code is uploaded to the Arduino board, and the PV cell temperature is recorded in an hourly basis. The PV cell temperature was recorded for several days with different weather conditions. The weather data such as solar radiation, ambient temperature, and wind speed corresponding to these days were obtained from the METU NCC weather station. Finally, PV cell temperature

estimations were made using this weather data. The predicted PV cell temperature is compared to the measured PV cell temperature to assess the performance of the predictions models and choose the most appropriate model.

Figure 3.13 PV module adjustable base

## 3.3 Soiling Analysis

Soiling has a detrimental effect on the performance and the degradation of PV modules. The intensity of its effect differs according to the installation and environmental conditions close to the modules. Modules with accumulated dust layers on the front surface experience sunlight attenuation and therefore significant power losses occur. Different types of dust in different environments have varying effects on the attenuation of sunlight due to the dust layers. This is according to the chemical properties and the physical properties of the dust such as the dust particle size. In this section, the methodology followed to investigate the effect of soiling on the performance of PV modules is discussed. The study aims to find the power loss due to soiling and estimate the total power losses of the METU NCC solar power plant.

In this part of the study, a different setup was used to carry on the experiment. Dust samples were collected from the surrounding areas of the METU NCC solar power plant to analyze its effect when accumulated on the modules. Since different dust types have a different effect on the attenuation of sunlight by the dust layers, it was especially important to ensure that the dust used during the investigation was of the same type in the surrounding environment of the solar power plant. The equipment used for the soiling analysis are presented as follows:

- Monocrystalline silicon PV module (**Figure 3.8**)
- Digital multimeters (**Figure 3.14**)
- Rheostat (**Figure 3.15**)
- Digital balance


Figure 3.14 Digital multimeter


Figure 3.15 Rheostat

The PV module was first installed on the adjustable base shown in **Figure 3.13**. The tilt angle (β) used for the module is 30° as it is in the METU NCC power plant to mimic the power plant installation and keep the factors the same to generalize the results for the METU NCC solar power plant. This is especially important for the soiling analysis as the tilt angle has a significant effect on the accumulation of dust on PV modules as it determines the effect of gravity on the settling of dust as discussed in the literature.

A circuit is constructed to be able to measure the power as dust is accumulated on the PV module and find the power losses. To do this, two digital multimeters such as the one shown in **Figure 3.14** were used to measure the voltage and current when the module is exposed to sunlight. To control the current and avoid any damage to the equipment, the rheostat shown in **Figure 3.15** is used to provide resistance in the circuit. The PV module was connected in series with the ammeter to measure the current. The ammeter is then connected in series with one side of the rheostat. The other side of the rheostat is connected back to the PV module to create the circuit. Finally, the voltmeter is connected in parallel with the rheostat to measure the voltage. The circuit constructed is shown in **Figure 3.16**.

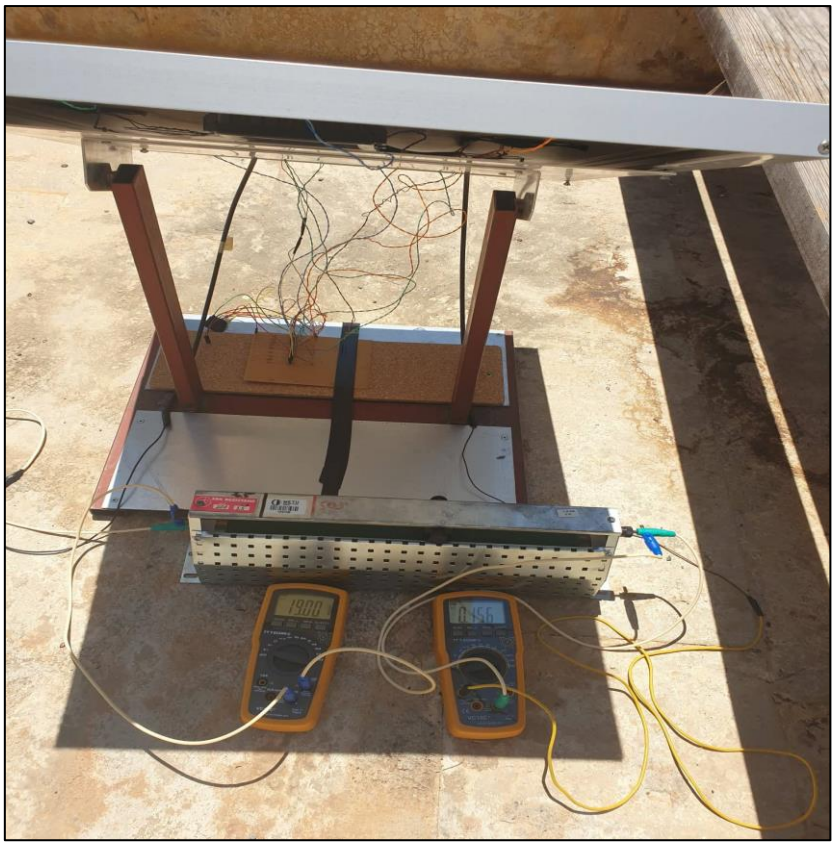

Figure 3.16 Circuit constructed for soiling analysis

After the circuit is constructed, the PV module is exposed to sunlight in an area close to the METU NCC power plant. The PV module was cleaned to ensure that no dust is accumulated on it before the experiment. The module was first exposed to sunlight for 15-30 minutes to reach thermal equilibrium with the surroundings. Then the voltage and the current of the circuit is measured to find the power. **Equation 3.27** was used to calculate the power.

$$P = I \times V \tag{3.27}$$

After finding the power generated by the clean module, dust was gradually accumulated on the front surface of the module in 5 g increments to reach the maximum of 30 g of accumulated dust as shown in **Figure 3.17**. A digital balance was used to weigh the dust samples used. At each increment, the voltage and current were measured to calculate the power and investigate the power loss. The power loss

percentage at each dust accumulation increment is found using **Equation 3.28** by comparing it to the power generated by the clean module.

$$Total\ power\ loss\ (\%) = \frac{P\ (clean\ module) - P\ (dusty\ module)}{P\ (clean\ module)} \times 100 \qquad (3.28)$$

The experiment was repeated for different ranges of solar irradiance to investigate the effect of soiling at different solar irradiance levels. The experiment was repeated in the exact same manner and the power losses were recorded to compare the power losses at different solar irradiance levels.

Figure 3.17 PV module with 30 g of dust accumulated on the front surface

# CHAPTER 4

# RESULTS AND DISCUSSION

## 4.1 PV Cell Temperature and Energy Production Predictions

In this section, the PV cell temperature predictions using nine different prediction models are compared to assess the accuracy of the models and find the most suitable prediction model for Northern Cyprus weather conditions. Accordingly, the energy production is also predicted and compared to the actual energy production. The PV cell temperature was measured throughout the study period as mentioned in **Section 3.2** to be compared to the predictions. The required data for the predictions are the solar irradiance, ambient temperature, and wind speed. The solar irradiance was obtained from the METU NCC weather station. At the time of the study, the ambient temperature and wind speed data were not available from the METU NCC weather station therefore was obtained from the nearest weather station.

After the PV cell temperature measurements were ready, and the required prediction data was gathered, the PV cell temperature predictions were made using Microsoft Excel as mentioned in **Section 3.1**. The specifications of the PV module used for the experiment can be found in **Appendix C.** Nine of the most commonly used PV cell temperature prediction models found in the literature (**Section 2.1**) were investigated to assess their accuracy for Northern Cyprus and are presented as follows:

- Sandia National Laboratory Model 1 (SNL 1)
- Sandia National Laboratory Model 2 (SNL 2)
- Mattei Energy Balance Model 1 (Mattei 1)
- Mattei Energy Balance Model 2 (Mattei 2)
- Skoplaki Wind Integrated NOCT Model 1 (Skoplaki 1)
- Skoplaki Wind Integrated NOCT Model 2 (Skoplaki 2)

- Faiman Hottel-Whillier-Bliss Equation Model (Faiman)
- Simple Linear Model (SLM)
- Nominal Operating Cell Temperature Model (NOCT)

The root mean squared error (RMSE) was used as in **Equation 3.22** to assess the accuracy of the PV cell temperature predictions over all the range of data gathered. According to the PV cell temperature predictions, the energy production was also computed, and the relative error (RE) was used as in **Equation 3.23** to assess the accuracy of the energy production prediction. The results of all the cell temperature and energy production predictions were compared to actual values that were measured throughout the duration of the study. The RMSE and the RE of all of the prediction models are presented in **Table 4.1**.

Table 4.1 RMSE and the RE of the PV cell temperature estimation models

| Model | RMSE (°C) | RE (%) |
|---|---|---|
| SNL 1 | 4.94 | 0.96 |
| SNL 2 | 5.88 | 2.11 |
| Mattei 1 | 4.84 | 0.38 |
| Mattei 2 | 4.68 | 0.43 |
| Skoplaki 1 | 4.34 | 0.01 |
| Skoplaki 2 | 4.51 | 1.21 |
| Faiman | 4.36 | 0.10 |
| SLM | 6.51 | 3.09 |
| NOCT | 9.43 | 4.46 |

In several studies found in the literature, it was indicated that an RMSE value of 5 °C and below is within an acceptable range of accuracy. Nevertheless, many studies have used the above-mentioned PV cell temperature prediction models and successfully predicted the cell temperature with an RMSE of 1-3 °C. The RMSE values obtained and shown in **Table 4.1** show an acceptable RMSE for most of the models investigated although it was expected to have lower RMSE values. This is due to a few reasons. Firstly, when a PV cell temperature prediction model is developed, some specific conditions such as the ambient temperature, wind speed, solar irradiance are assumed, and experimentations are carried on to empirically

develop the models. Any significant differences between the conditions assumed by the model and the conditions of prediction may result in accuracy problems therefore it is important to find the most appropriate prediction models according to the location. Results with higher RMSE values compared to the literature may indicate that these models are not appropriate or sufficiently accurate to be used for PV cell temperature predictions in Northern Cyprus weather conditions due to the variation from the assumed conditions of the models.

Nevertheless, this brings the discussion to the second point which is that some of the weather data used for the predictions were not obtained from the exact same location where the experiments were conducted. This was mainly due to the insufficient availability of data and apparatus for some of the measurements needed. As explained in **Section 3.1**, the total solar irradiance has 3 main components which include the beam, diffuse, and reflected irradiance. Each component of solar irradiance has specific measurement apparatus used for measurements. To be able to find the total solar irradiance incident on a tilted surface (surface of the PV module), the global solar radiation and the beam normal radiation measurements are required for calculations. The global solar radiation which represents the total solar radiation incident on a horizontal surface was obtained from the METU NCC weather station. However, the beam normal radiation which represents the beam insolation parallel to sun rays (DNI) requires the use of a pyrheliometer with tracker and was not available at the time of the study. To compensate for this, typical meteorological year (TMY) values of the DNI were obtained and used in the calculations instead. This has affected the values of the solar irradiance incident on the module therefore affecting the accuracy of the predictions.

Furthermore, the ambient temperature and the wind speed data were not available throughout the study period at the exact location of the experiment. To compensate for this, data from the Ercan Airport weather station was used which was the nearest weather station with readily available weather data. The ambient temperature has a direct effect on the PV cell temperature due to free convection. The wind speed also has a significant effect on the PV cell temperature as it causes the cooling of the PV

module through forced convection and must not be ignored according to several studies in the literature (**Section 2.1**). Ignoring the wind speed for PV cell temperature predictions causes the predictions to be higher than actual values. All of the above-mentioned factors have clearly affected the predictions therefore the RMSE values obtained for all of the prediction models are generally higher than expected. Ideally, weather data must be obtained from the exact location of the experiment to produce accurate cell temperature predictions and investigate the models.

Regardless of the limitations mentioned above, the performances of the PV cell temperature prediction models were compared to investigate the most appropriate model for Northern Cyprus weather conditions. **Figure 4.1** shows the measured and predicted PV cell temperature values with respect to the hour of day. A line of best fit was used for the data points of the predictions to show a general trendline to be compared to the measurements. The time of the day which was covered in the study is from the $10^{th}$ hour of the day until the $20^{th}$ hour of the day which is from 9 AM until 7 PM. It is observed that all of the models have shown a trendline matching with the measured values and most of the models show a trendline within the range of measured values.

The RMSE represents the quantifies the overall deviation of the predictions from the measurements shown in **Figure 4.1**. Judging by the RMSE values presented in **Table 4.1**, the top three predictions models for Northern Cyprus weather conditions based on their accuracy are Skoplaki 1, followed by Faiman, followed by Skoplaki 2. The RMSE values of all the models are expected to be even lower if data at the exact location was available and used for the predictions.

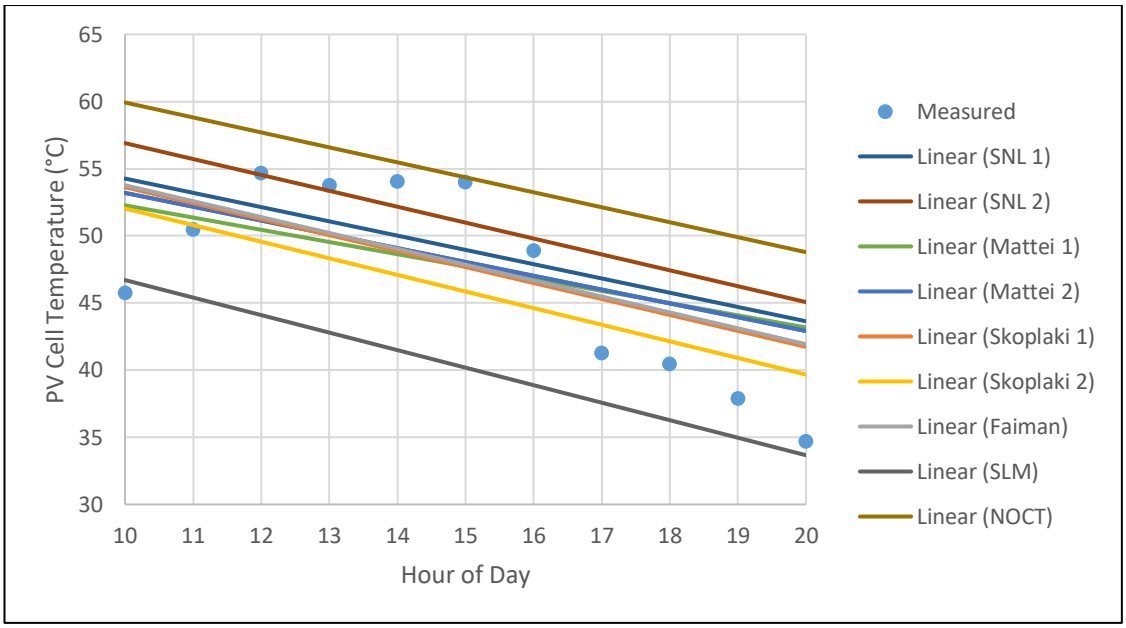


Figure 4.1 Measured and predicted PV cell temperature vs hour of the day

After predicting the PV cell temperature as indicated above, the energy production was accordingly predicted as mentioned in **Section 3.1**. The relative error (RE) of the energy productions predictions resulting from the PV cell temperature predictions by the models is shown in **Table 4.1**. It is observed that although the RMSE of the models is relatively high, the energy generation predictions are very accurate within an acceptable range. **Figure 4.2** shows the actual and predicted hourly total energy production with respect to the time of day. It is observed that all of the energy production predictions generally match the measurements as they show the exact same shape of the graph to an extent that many of the lines override each other. According to the RE values of the energy production predictions by the models that are shown in **Table 4.1**, the top 3 most accurate models are Skoplaki 1, followed by Faiman, followed by Mattei 1 with RE values of 0.01%, 0.1%, and 0.38% respectively. Considering both the RMSE and the RE, Skoplaki 1 is the most appropriate model to be used for PV cell temperature prediction and energy production prediction for Northern Cyprus weather conditions.

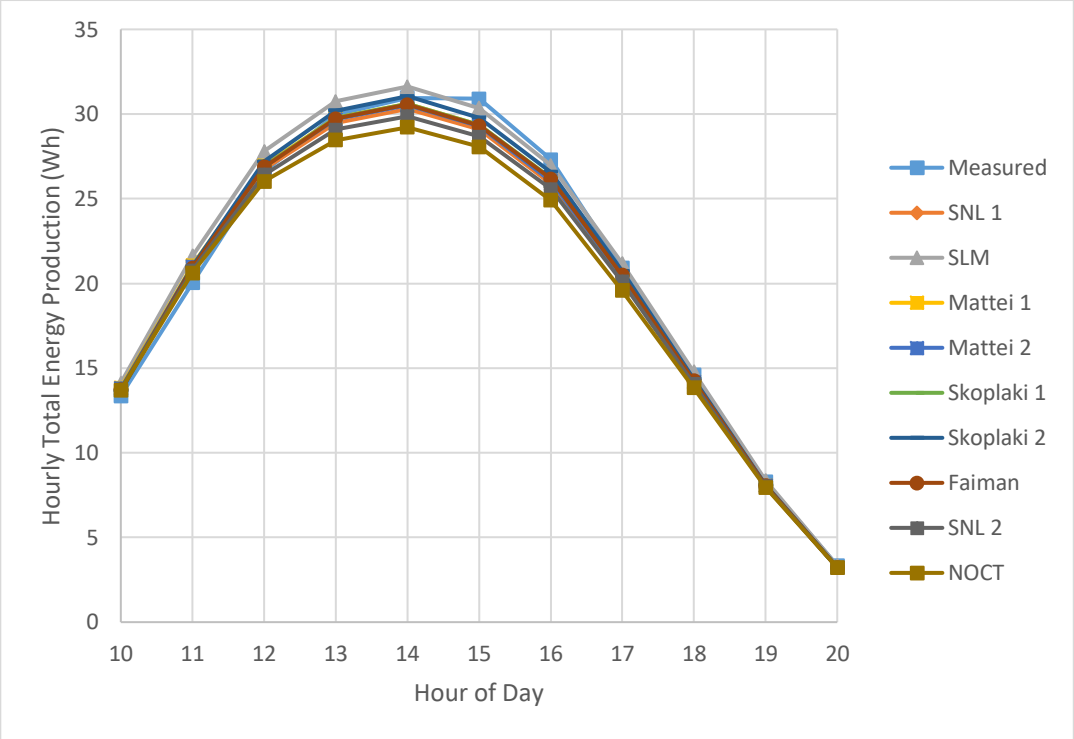


Figure 4.2 Measured and predicted hourly total energy production vs hour of day

## 4.2 Soiling Analysis

In this section, the result of the soiling analysis is discussed. The soiling analysis was conducted on a PV module with similar specifications and orientation as in the METU NCC solar power with the purpose of generalizing the results and scaling it to the solar plant. Dust samples were obtained from the surroundings and was accumulated on the module in 5g increments to reach a total of 30g of accumulated dust on the front surface of the module as mentioned in **Section 3.3**. A circuit was constructed to measure the voltage and the current to be able to calculate the output power at every increment of dust accumulation starting from a clean module until 30g of dust is accumulated. At every stage the total power loss was calculated as a percentage compared to the power output of the clean module.

The experiment was repeated for different ranges of solar irradiance to investigate the power losses. The ranges of solar irradiance investigated are 100-300 $W/m^2$,

300-500 $W/m^2$, 500-700 $W/m^2$, 700-900 $W/m^2$, and 900-1000 $W/m^2$. The power losses at each mass of dust accumulated on the module at each irradiance range investigated are presented in **Figures 4.3-4.7**. It is observed from all the figures that as the amount of dust accumulated on the module increases, the power output of the modules decrease too which is what is expected. This shows that as the dust deposition density increases, the attenuation of sunlight from the dust layer increases causing significant power losses. Maximum power losses of 12-15% were observed at 30g of dust accumulated on the module in Northern Cyprus weather conditions.

At lower irradiance levels of 100 $W/m^2$ until irradiance levels of 700 $W/m^2$, it is observed that the greatest power loss in terms of percentage occurs at the last increment of total 30g accumulated dust as the graph is the steepest between 25g of dust and 30g of dust as seen in **Figures 4.3-4.5**. On the other hand, the effect of 5g and 10g of accumulated dust is less significant as the graph is less steep withing these dust amounts. At higher irradiance levels of 700 $W/m^2$ an above, it is observed from **Figures 4.6-4.7** that the greatest power loss occurs at the increment of 15g of dust accumulated as it is where the graph is the steepest. Any more dust accumulated after 15g causes a relatively constant rate of increase in power loss.

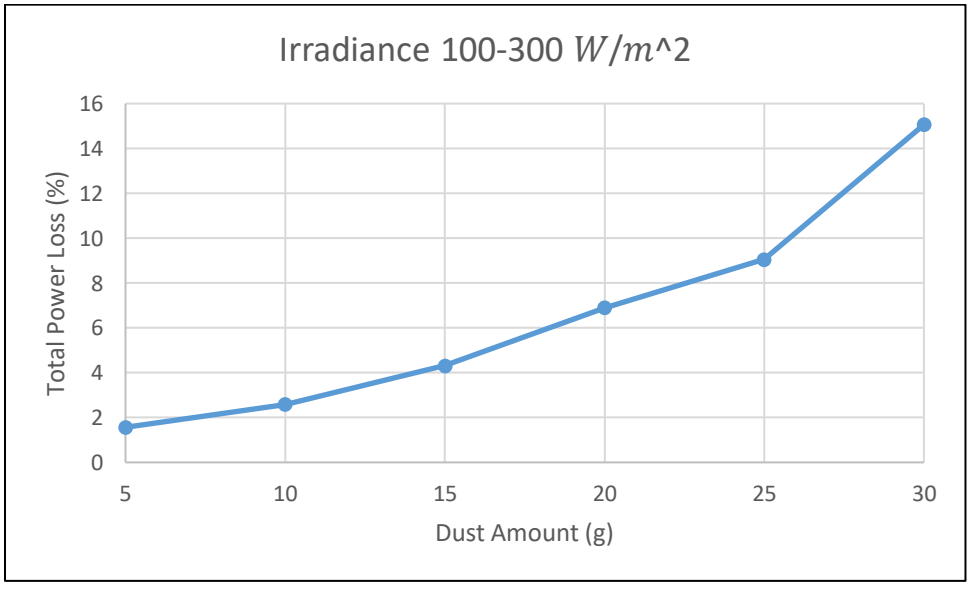


Figure 4.3 Total power loss vs dust amount accumulated for solar irradiance levels of 100-300 $W/m^2$

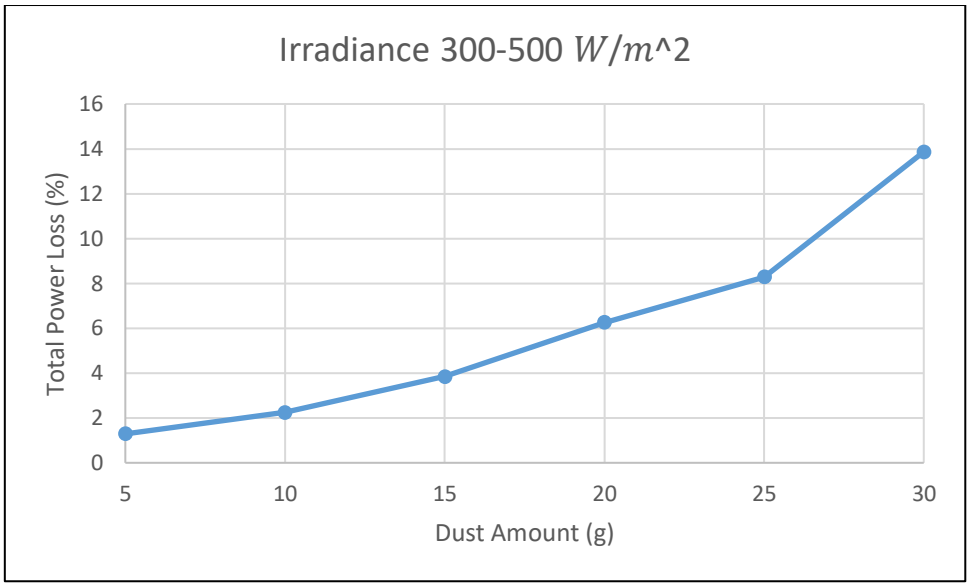


Figure 4.4 Total power loss vs dust amount accumulated for solar irradiance levels of 300-500 $W/m^2$

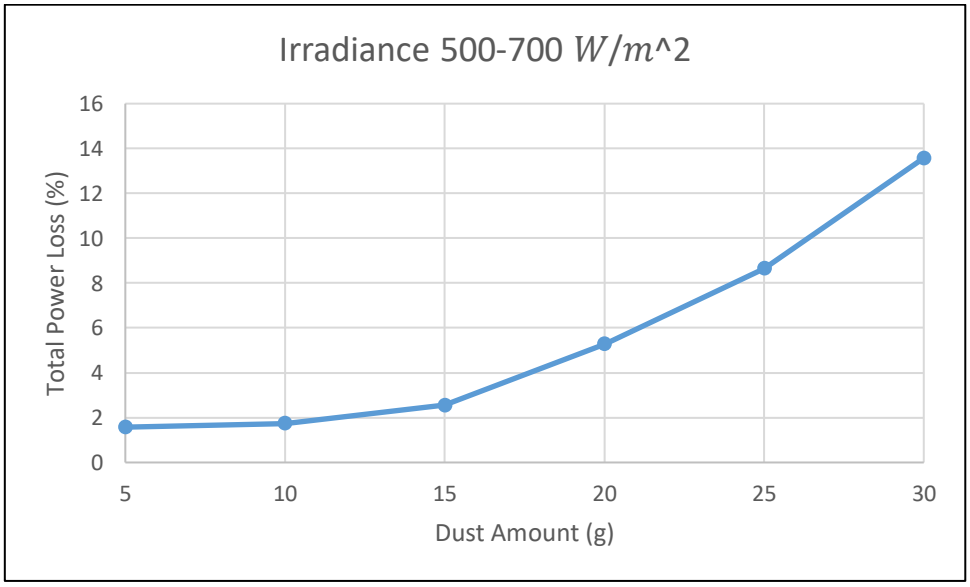


Figure 4.5 Total power loss vs dust amount accumulated for solar irradiance levels of 500-700 $W/m^2$

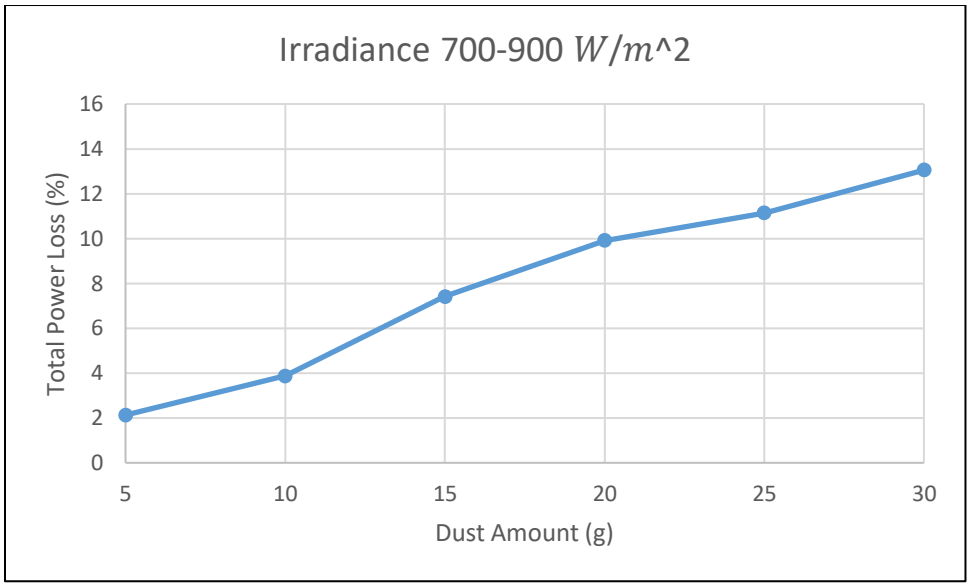


Figure 4.6 Total power loss vs dust amount accumulated for solar irradiance levels of 700-900 $W/m^2$

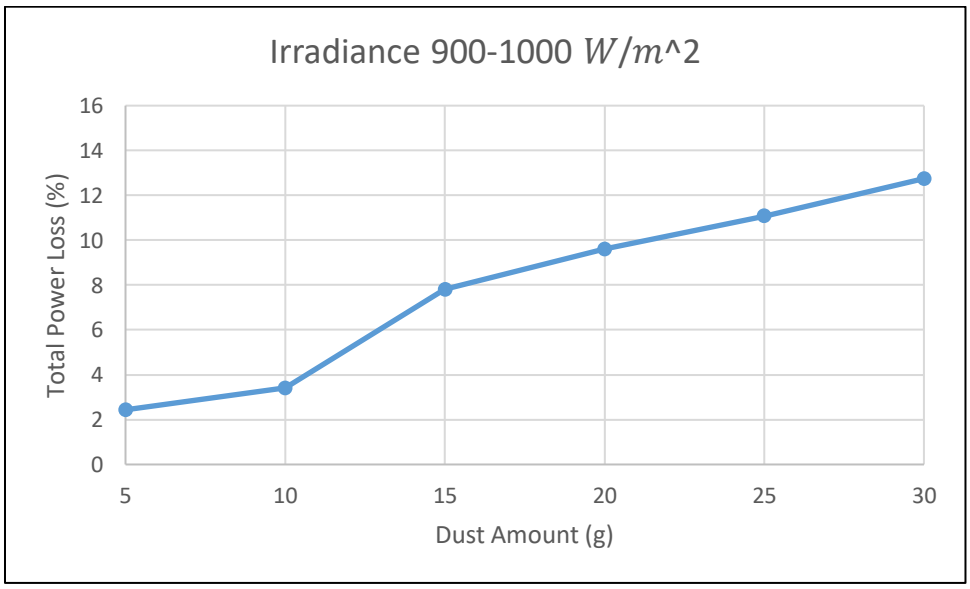


Figure 4.7 Total power loss vs dust amount accumulated for solar irradiance levels of 900-1000 $W/m^2$

Furthermore, the effect of dust on the performance of PV modules and more specifically the power losses at different irradiance levels is compared. **Figure 4.8** shows the maximum power loss at 30g of accumulated dust for each irradiance level investigated. The maximum power loss of 15% has occurred at 100-300 $W/m^2$ whereas a maximum power loss of 12.7% has occurred at 900-1000 $W/m^2$. It is observed that as the solar irradiance decreases, the maximum output power loss increases. This shows that the effect of soiling on the performance of PV modules and more specifically the attenuation of sunlight by the dust layer is more significant at lower irradiance levels. When the irradiance level is low, and the dust deposition density is high, a condition arises where there is low sunlight availability in the atmosphere alongside significant sunlight attenuation by the dust layer resulting in a greater maximum power loss.

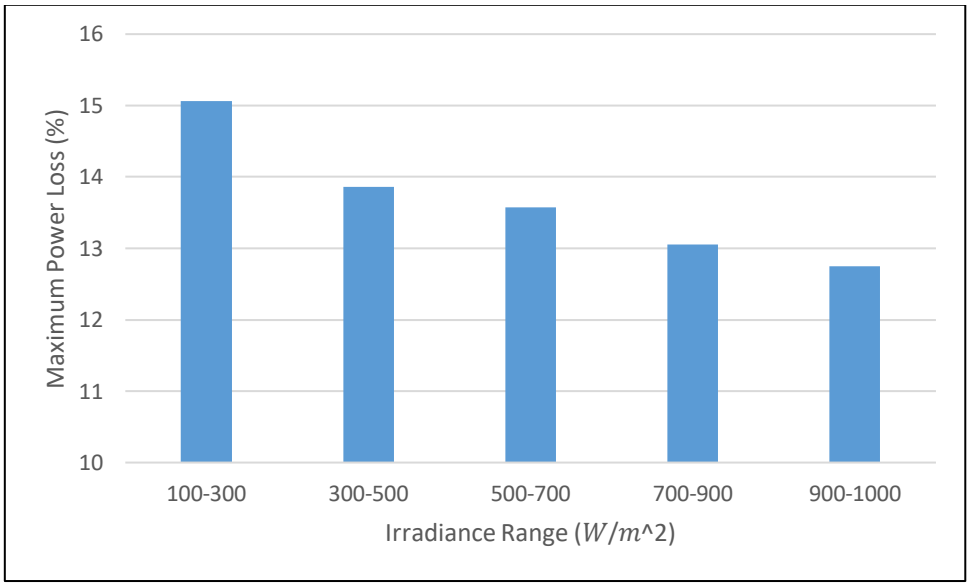


Figure 4.8 Maximum power loss at 30g of dust accumulated at each solar irradiance range investigated

The PV module used during the soiling investigation has lost around 12.7% of the power output with 30g of dust was accumulated when compared to the power output of the clean module at the solar irradiance range of 900-1000 $W/m^2$. The area of the module used in the experiment is 0.34 $m^2$. Depositing 30 g of dust on a 0.34 $m^2$ module is equivalent to a dust deposition density of 88 $g/m^2$. The METU NCC

power plant has a 1 MW capacity. It consists of 4000 PV modules that are 250W each. The area of a single module is 1.63 $m^2$ making the total area of the solar plant about 6520 $m^2$. At the time of the study, the solar power plant produces around 400 kW at around 1000 $W/m^2$ solar irradiance when the modules are clean. Assuming that 88 $g/m^2$ are accumulated over time on the modules in the power plant, a power loss of 51 kW is expected at the 900-1000 $W/m^2$ solar irradiance range if the modules were not cleaned. This is a significant amount of power loss that over time reduces the total energy yield from the solar power plant on top of further module overheating and degradation issues that may be caused by dust.

An important thing to note is that while performing the soiling experiments and adding dust to the modules, a dust deposition/settling system was not available therefore the dust was accumulated manually. This causes the dust to be distributed in a non-uniform way potentially causing clean spots and an uneven settling of the dust. This has implications that decreased the sunlight attenuation effect by the dust layers as more sunlight can reach the module through the relatively clean spots. This means that the expected power losses at 88 $g/m^2$ are expected to be more than 12.7%. The dust deposition density of 88 $g/m^2$ is relatively high and would be very rare to naturally occur. Although it is rare, it is expected that a lower dust deposition density that is possible to occur naturally will cause a similar power loss if not more when accumulated in a uniform way.

To further validate the results, a real scenario from the METU NCC solar power plant was investigated. The total power output of the clean solar power plant at 1000 $W/m^2$ was compared to the power output of the solar power plant immediately before cleaning. **Figure 4.9** shows the power output of the solar power plant on the 19$^{th}$ of June 2022 where the plant has not been cleaned for a while. As observed from the figure, the maximum power output of the solar power plant was about 300 kW at the irradiance level of 1000 $W/m^2$. On the 20$^{th}$ of June 2022, the solar power plant was cleaned from all residue and dust on the PV modules. **Figure 4.10** shows the power output of the solar power plant on the 21$^{st}$ of June 2022 where the plant was

completely cleaned. It is observed from the figure that the solar power plant has produced a maximum power output of 400kW at the solar irradiance of 1000 $W/m^2$. The difference in power output between the plant before and after cleaning has shown about 25% power loss at the irradiance level of 1000 $W/m^2$. This highlights the effect of soiling on the performance of PV modules and highlights the importance of regular cleaning to avoid such significant power losses.

Another important observation is that although the results of the soiling study conducted has shown a maximum power loss of 12.7% for the dust deposition density of 88 $g/m^2$ at the solar irradiance level of 1000 $W/m^2$, it is highly unlikely that the solar power plant had such a high dust deposition density before cleaning since this dust deposition density is very rare to occur naturally outdoors due to wind, rain, and other outdoor climatic conditions. This results in two main conclusions. Firstly, that a dust deposition density lower than 88 $g/m^2$ has caused about 25% power loss therefore the power losses found in the results are lower than expected. Secondly, it highlights the importance of ensuring uniform dust distribution when investigating the effect of soiling on the performance of PV modules.

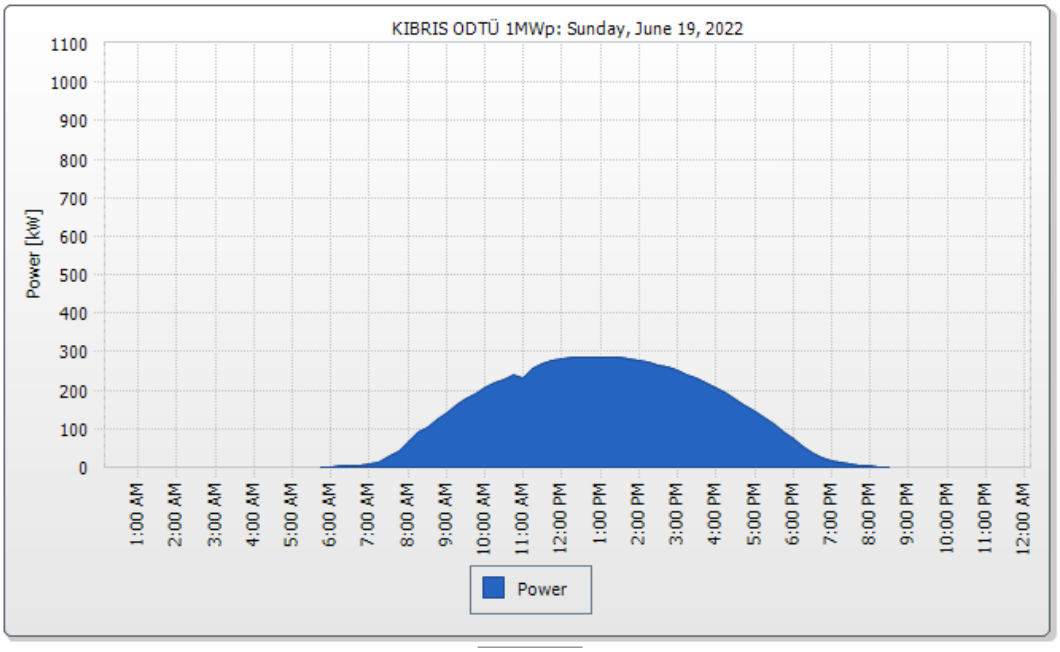


Figure 4.9 Power output of the METU NCC solar power plant before cleaning

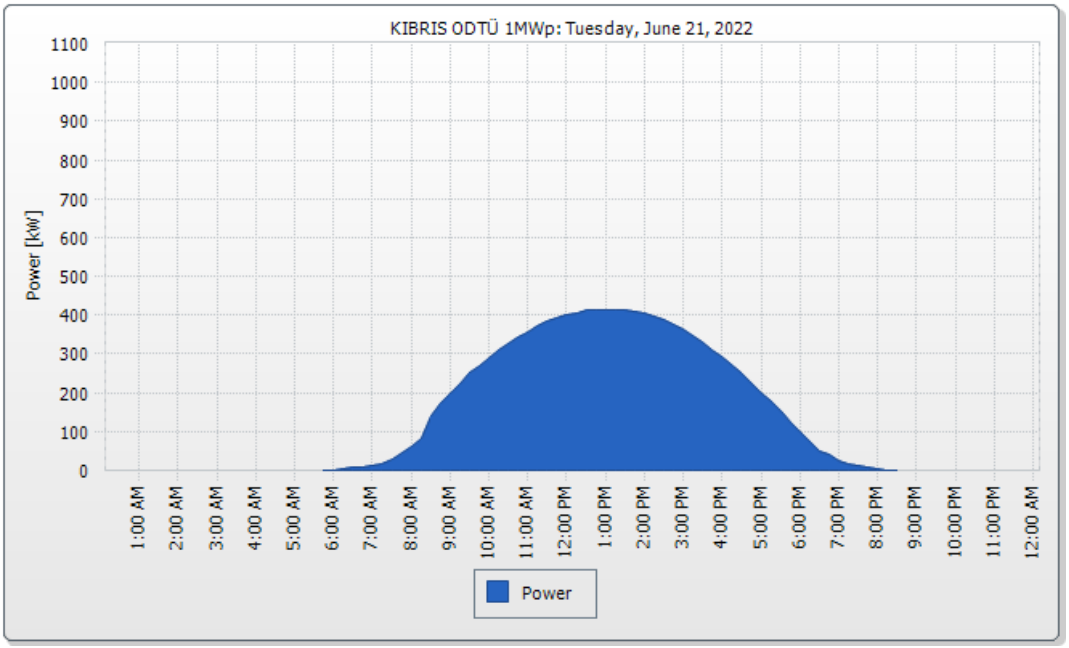


Figure 4.10 Power output of the METU NCC solar power plant after cleaning

After the power plant has been cleaned, a 25% percent power loss due to soiling was observed when comparing before and after cleaning. The cleaning was done on the 20th of June 2022. **Figure 4.11** shows the power output of the solar power plant on the 22nd of August 2022 two months after the cleaning was done. As observed from the figure, the maximum power output is about 350 kW at the solar irradiance level of 1000 $W/m^2$ indicating a power loss of 12.5% compared to the power output of the clean solar power plant. This further illustrates the importance of regular cleaning and how as dust accumulates on the modules, the power output gradually decreases. Another important observation is that the months that were considered for this investigation (June-August) are dry summer months where almost no rainfall has occurred. The power losses in the winter season where more rainfall occurs is expected to be less as rainfall cleans the modules. It is especially more important to observe the regular cleaning of the solar power plant during the dry summer months and generally throughout the whole year. The minimum cleaning frequency recommended for regions of Mediterranean climate such as Northern Cyprus is once every 2 weeks (Mani & Pillai, 2010).

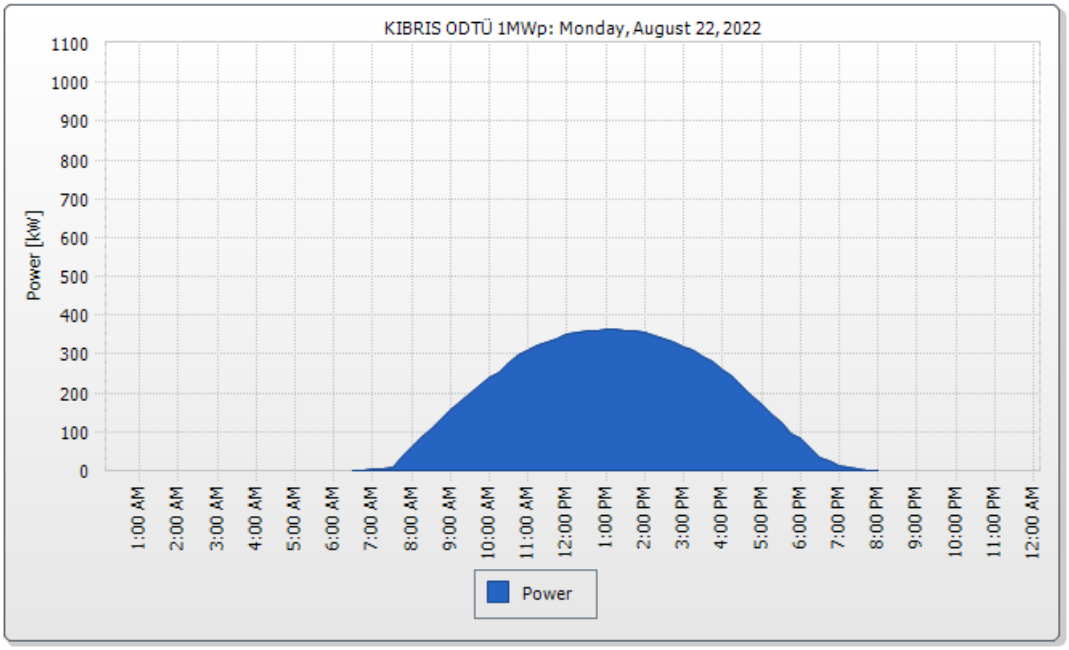


Figure 4.11 Power output of the METU NCC solar power plant two months after cleaning

It is important to note a few things related to the above mentioned results. Firstly, these results cannot be generalized elsewhere as they are case specific. The effect of soiling on the performance of PV modules depends on many factors that were mentioned in detail **Section 2.3**. Nevertheless, factors such as environmental conditions, module tilt angle, and the type of dust available in a region determine how significant the effect of soiling is on the performance of a PV module. Since this investigation was carried out in Northern Cyprus, and the dust samples used were gathered from nearby surrouundings, the power losses are very specific to this area only. Secondly, a solar simulator was not available therefore the experiment was done outdoors within a small time range to be able to ensure that the solar irradiance stays at the desired levels of expermintation. Thirdly, a dust deposition system was not available to ensure the uniform distribution of dust on the PV module. The uniform distribution of dust causes further attenuation of sunlight as there would be no empty spots for sunlight to go through to reach the module. With that said, the power losses observed from this soinling experiment are less than the expected power losses at the respective dust deposition amounts. Finally, to be able to further

generalize the results, it is important to analyse the dust type and more specifically the chemical and physical properties of the dusts samples gathered as different types of dust have different effects on the perfomance of PV modules and its corresponding power losses. Some types of dust even cause the degradation of and damage to the PV modules.

# CHAPTER 5

# CONCLUSION

In this thesis, nine different PV cell temperature prediction models were compared to assess the accuracy of the models and find the most suitable prediction model for Northern Cyprus weather conditions. Accordingly, the energy production was also predicted using the predicted cell temperatures and was compared to the actual energy production. PV cell temperature measurements were made through the duration of the study to be able to assess the accuracy of the models by comparing predicted and measured values. The root mean square error (RMSE) was used for the PV cell temperature predictions while the relative error was used for the resulting energy production predictions.

The most accurate models in predicting the PV cell temperature were Skoplaki 1, Faiman, and Skoplaki 2 respectively with a RMSE of 4.34 °C, 4.36 °C, and 4.51 °C respectively. Compared to other studies in the literature, these RMSE values are relatively high. This is mainly because there was a shortage in data needed in the prediction at the exact specific location including solar irradiance, wind speed, and ambient temperature. To compensate this, the data that was not available from the METU NCC weather station was either replaced by typical meteorological year (TMY) data or obtained from the nearest weather station which was at Ercan airport. This has affected the accuracy of the predictions therefore the RMSE values were higher than expected. If the experiments are repeated with the necessary weather data at the exact location of the study, the RMSE values are expected to be lower, and the results would be further verified.

The total energy production was also predicted using the PV cell temperature predictions. The models with the lowest relative errors were Skoplaki 1, followed by Faiman, followed by Mattei 1 with RE values of 0.01%, 0.1%, and 0.38%

respectively. Considering both the RMSE and the RE, Skoplaki 1 is the most appropriate model to be used for PV cell temperature prediction and energy production prediction for Northern Cyprus weather conditions.

Another part of this thesis was to conduct a soiling analysis to investigate the effect of dust on the performance PV modules in Northern Cyprus weather conditions. Dust samples were obtained from the surroundings and was accumulated on the module in 5g increments to reach a total of 30g of accumulated dust on the front surface of the module. A circuit was constructed to measure the voltage and the current to be able to calculate the output power at every increment of dust accumulation starting from a clean module until 30g of dust is accumulated. 30 g of dust accumulated on the module used in the experiment is equivalent to 88 $g/m^2$ of dust deposition density. At every stage the total power loss was calculated as a percentage compared to the power output of the clean module. The experiment was repeated over several solar irradiance ranges to further investigate the power losses. It was found that the maximum power losses after accumulating 30g (88 $g/m^2$) of dust on the module were ranging from 12.75-15% at different irradiance levels. It was also found that at lower irradiance levels, the attenuation of sunlight by the dust layers is more significant and has resulted in greater power losses as it creates a scenario where low sunlight is available in addition to the attenuation of sunlight effect by the dust layer.

To further verify the previous soiling analysis results, a real scenario from the METU NCC solar power plant has been investigated. A maximum power loss of 25% at the irradiance level of 1000 $W/m^2$ was observed from the solar power plant when comparing the power output before and after cleaning the modules in the plant. The solar plant was not cleaned for a while before that comparison. The maximum power losses observed from the solar power plant are generally higher than the power losses found in the soiling experiment conducted which showed a maximum power loss of 12.75% at the same irradiance level with a dust deposition density of 88 $g/m^2$. This either means that the dust accumulated in the solar plant before cleaning was of higher dust deposition density or, the power losses at 88 $g/m^2$ of dust deposition

and 1000 $W/m^2$ are expected to be higher than the results found in the study which was only 12.75% at the same irradiance level compared to 25% in the solar power plant. Since the dust deposition density of 88 $g/m^2$ is very high, it is highly unlikely to have occurred naturally in the power plant especially since climatic conditions such as wind and rain provide natural cleaning for the module to an extent. With that said, it is concluded that the maximum power losses found in the soiling study are expected to be higher at the same irradiance levels and dust deposition density of 88 $g/m^2$. A lower dust deposition density has caused a greater power loss in the solar power plant.

The most likely reason for this error is that a dust deposition system was not available to distribute the dust uniformly on the module when conducting the study. The dust was accumulated manually in an ununiformed way which has created uneven spots that have affected the attenuation of sunlight by dust layer due to sunlight going through cleaner spots to reach the module. Dust settling on a PV module is naturally occurring in a more uniform way due to gravity causing more significant attenuation of sunlight therefore it is important to ensure the uniform distribution of dust to achieve more accurate results when conducting a soiling study.

The power output of the solar power plant when cleaned was also compared to the power output of the plant 2 months after the cleaning and a 12.5% maximum power loss was observed at the same irradiance level of 1000 $W/m^2$. This further highlights the importance of the regular cleaning of the modules to avoid such significant power losses. A minimum cleaning frequency of 2 times a week is recommended in the literature for regions of Mediterranean climate such as Northern Cyprus.

These results are specific to the dust available in Northern Cyprus and its weather conditions as the effect of soiling on the performance of PV modules depends on several factors such as the module orientation, environmental conditions, and the physical and chemical properties of the dust accumulated on the module. This soiling study illustrates the importance of the regular cleaning and maintenance of modules as these power losses are significant in the short and the long term.

# CHAPTER 6

## FUTURE WORK AND IMPROVEMENTS

- A thermal camera can be used to further verify the thermistor sensor temperature measurements and accordingly calibrate if needed.

- Since a data logger was not available at the time of the study, PV cell temperature measurements were recorded on an hourly basis. A data logger is to be used to be able to record cell temperature measurements on a minutely basis which would produce more accurate results and further verify the current results.

- Some weather data needed for the prediction of the PV cell temperature was not available at the time of the study. This is mainly solar irradiance, wind speed, and ambient temperature. To compensate for this typical meteorological year (TMY) data and data from another nearby weather station was used. This has affected the accuracy of the results. Further work can be done to obtain this data at the exact study location. This includes the beam normal radiation (DNI), wind speed close to the module, and ambient temperature close to the module. This data can be used to produce more accurate PV cell temperature predictions and further verify the current results.

- The PV cell temperature estimation methods have been investigated and their performance was verified by comparing estimations to measurements took during the summer. Further work can be done to investigate the accuracy of the models for other seasons which have different weather conditions. PV

cell temperature measurements may be obtained for the whole year and compared to estimations to find the best prediction models with respect to months and seasons.

- Dust deposition occurs naturally due to wind and gravity. A dust deposition system and a solar simulator may be used to more accurately assess the effect of dust on the performance of the PV system. Dust samples must be gathered from Northern Cyprus if it is the desired case to be studied.

- Different dust types with different particle sizes, physical properties, and chemical properties have a different effect on the sunlight attenuation by the dust layer and the overall performance of the PV module. Further experimental procedures may be done to investigate the types of dust available in Northern Cyprus to more accurately assess its effect on module performance.

- According to the properties of dust and the amount of dust accumulation in the region, the proper PV module cleaning method and cleaning frequency may be investigated.

## REFERENCES


Alonso García, M. C., & Balenzategui, J. L. (2004). Estimation of photovoltaic module yearly temperature and performance based on Nominal Operation Cell Temperature calculations. *Renewable Energy*, *29*(12), 1997–2010. https://doi.org/10.1016/j.renene.2004.03.010

Appels, R., Muthirayan, B., Beerten, A., Paesen, R., Driesen, J., & Poortmans, J. (2012). The effect of dust deposition on photovoltaic modules. *Conference Record of the IEEE Photovoltaic Specialists Conference*, 1886–1889. https://doi.org/10.1109/PVSC.2012.6317961

Ballinger Jr, K. E. (2001). *Method of deterring birds from plant and structural surfaces. U.S. Patent No. 6,328,986. Washington, DC: U.S. Patent and Trademark Office.*

Bardhi, M., Grandi, G., & Tina, G. M. (2012). Comparison of PV cell temperature estimation by different thermal power exchange calculation methods. *Renewable Energy and Power Quality Journal*, *1*(10), 653–658. https://doi.org/10.24084/repqj10.417

Cabanillas, R. E., & Munguía, H. (2011). *Dust accumulation effect on efficiency of Si photovoltaic modules. Journal of Renewable and Sustainable Energy, 3(4), 043114.*

Charles Lawrence, W. K., Rok Lim, J., Sub Won, C., & Ahn, H. (2017). *Prediction Model of Photovoltaic Module Temperature for Power Performance of Floating PVs*. https://doi.org/10.20944/preprints201712.0094.v1

Dayan, U., Ziv, B., Shoob, T., & Enzel, Y. (2008). Suspended dust over southeastern Mediterranean and its relation to atmospheric circulations. *International Journal of Climatology*, *28*(7), 915–924. https://doi.org/10.1002/joc.1587

Duffle, John, & Beckman. (2006). *Solar Energy Thermal Processes, third ed. Wiley, Hoboken, NJ, 23.3.* .

Elminir, H. K., Ghitas, A. E., Hamid, R. H., El-Hussainy, F., Beheary, M. M., & Abdel-Moneim, K. M. (2006). Effect of dust on the transparent cover of solar collectors. *Energy Conversion and Management*, *47*(18–19), 3192–3203. https://doi.org/10.1016/j.enconman.2006.02.014

El-Shobokshy, M. S., & Hussein, F. M. (1993). *Effect of dust with different physical properties on the performance of photovoltaic cells. Solar energy, 51(6), 505-511.*

Faiman, D. (2008). Assessing the outdoor operating temperature of photovoltaic modules. *Progress in Photovoltaics: Research and Applications*, *16*(4), 307–315. https://doi.org/10.1002/pip.813

Gaier, J. R., & Perez-Davis, M. E. (1991). *Effect of particle size of Martian dust on the degradation of photovoltaic cell performance. In International Solar Energy Conference (No. E-6556).*

Gavin Mangeni, Rodney Tan, T. Tan, S. Cheo, v. Mok, & J. Pang. (2017). *$I^2$MTC 2017 IEEE International Instrumentation and Measurement Technology Conference : Photovoltaic Module Cell Temperature Measurements using Linear Interpolation Technique, 2017, Politecnico di Torino, Torino, Italy*.

Haeberlin, H., Graf, J. D., & Fachhochschule, B. (1998). Gradual Reduction of PV Generator Yield due to Pollution. In *2 nd World Conference on Photovoltaic Solar Energy Conversion*.

Hammond, R., Srinivasan, D., Harris, A., Whitfield, K., & Wohlgemuth, J. (1997). *Effects of soiling on PV module and radiometer performance. In Conference Record of the Twenty Sixth IEEE Photovoltaic Specialists Conference-1997 (pp. 1121-1124). IEEE.*

Hegazy, A. A. (2001). Effect of dust accumulation on solar transmittance through glass covers of plate-type collectors. In *Renewable Energy* (Vol. 22). www.elsevier.nl/locate/renene

Hinds, W., & Zhu, Y. (1999). *Aerosol technology: properties, behavior, and measurement of airborne particles. John Wiley & Sons.*

Hoffman, A. R. (1980). *Photovoltaic module soiling studies May 1978-October 1980 (Vol. 80). Jet Propulsion Laboratory, California Institute of Technology.*

Jovanović, U., Mančić, D., Jovanović, I., & Petrušić, Z. (2017). Temperature measurement of photovoltaic modules using non-contact infrared system. *Journal of Electrical Engineering and Technology*, *12*(2), 904–910. https://doi.org/10.5370/JEET.2017.12.2.904

Ju, X., Vossier, A., Wang, Z., Dollet, A., & Flamant, G. (2013). An improved temperature estimation method for solar cells operating at high concentrations. *Solar Energy*, *93*, 80–89. https://doi.org/10.1016/j.solener.2013.02.028

Kaldellis, J. K., Fragos, P., & Kapsali, M. (2011). *Systematic experimental study of the pollution deposition impact on the energy yield of photovoltaic installations. Renewable energy, 36(10), 2717-2724.*

King, D. L., Boyson, W. E., & Kratochvill, J. A. (2004). *SANDIA REPORT Photovoltaic Array Performance Model*. http://www.ntis.gov/help/ordermethods.asp?loc=7-4-0#online

Koehl, M., Heck, M., Wiesmeier, S., & Wirth, J. (2011). Modeling of the nominal operating cell temperature based on outdoor weathering. *Solar Energy Materials and Solar Cells*, *95*(7), 1638–1646. https://doi.org/10.1016/j.solmat.2011.01.020

Kurtz, S., Whitfield, K., Miller, D., Joyce, J., Wohlgemuth, J., Kempe, M., Dhere, N., Bosco, N., & Zgonena, T. (2009). Evaluation of high-temperature exposure of rack-mounted photovoltaic modules. *Conference Record of the*

*IEEE Photovoltaic Specialists Conference*, 002399–002404. https://doi.org/10.1109/PVSC.2009.5411307

Lamont, L. A., & el Chaar, L. (2011). *Enhancement of a stand-alone photovoltaic system's performance: Reduction of soft and hard shading. Renewable energy, 36(4), 1306-1310.*

Lasnier, & Ang. (1990). *Photovoltaic Engineering Handbook. Adam Hilger, New York, NY, p.80.*

Mani, M., & Pillai, R. (2010). Impact of dust on solar photovoltaic (PV) performance: Research status, challenges and recommendations. In *Renewable and Sustainable Energy Reviews* (Vol. 14, Issue 9). Elsevier Ltd. https://doi.org/10.1016/j.rser.2010.07.065

Mattei, M., Notton, G., Cristofari, C., Muselli, M., & Poggi, P. (2006). Calculation of the polycrystalline PV module temperature using a simple method of energy balance. *Renewable Energy*, *31*(4), 553–567. https://doi.org/10.1016/j.renene.2005.03.010

Mekhilef, S., Saidur, R., & Kamalisarvestani, M. (2012). Effect of dust, humidity and air velocity on efficiency of photovoltaic cells. In *Renewable and Sustainable Energy Reviews* (Vol. 16, Issue 5, pp. 2920–2925). https://doi.org/10.1016/j.rser.2012.02.012

Molki, A. (2010). *Dust Affects Solar-Cell Efficiency. Physics Education, 45(5), 456-458.*

Muzathik, A. M., & Muzathik, A. M. (2014). *Photovoltaic Modules Operating Temperature Estimation Using a Simple Correlation* (Vol. 4). https://www.researchgate.net/publication/267911000

Nahar, N. M., & Gupta, J. P. (1990). *Effect of dust on transmittance of glazing materials for solar collectors under arid zone conditions of India. Solar & wind technology, 7(2-3), 237-243.*

Nathan Guay, Cliffor Hansen, Charles Robinson, & Bruce King. (2016). *2016 IEEE 43rd Photovoltaic Specialists Conference (PVSC)*. IEEE.

Nishioka, K., Miyamura, K., Ota, Y., Akitomi, M., Chiba, Y., & Masuda, A. (2018). Accurate measurement and estimation of solar cell temperature in photovoltaic module operating in real environmental conditions. *Japanese Journal of Applied Physics*, *57*(8). https://doi.org/10.7567/JJAP.57.08RG08

Rauschenbach. (1980). *Solar cell array design handbook-The principles and technology of photovoltaic energy conversion. NASA STI/Recon Technical Report A, 80, 34847.*

Risser, & Fuentes. (1984). *Linear regression analysis of flat-plate photovoltaic system performance data. In 5th Photovoltaic Solar Energy Conference (pp. 623-627).1984.*

Ross Jr. (1976). *Interface design considerations for terrestrial solar cell modules. In 12th Photovoltaic specialists conference (pp. 801-806).*

Salim, A. A., Huraib, F. S., & Eugenio, N. N. (1988). *PV power-study of system options and optimization. In EC photovoltaic solar conference. 8 (pp. 688-692).*

Sayyah, A., Horenstein, M. N., & Mazumder, M. K. (2014). Energy yield loss caused by dust deposition on photovoltaic panels. *Solar Energy*, *107*, 576–604. https://doi.org/10.1016/j.solener.2014.05.030

Schott. (1985). *Operation temperatures of pv modules: a theoretical and experimental approach. In EC Photovoltaic solar energy conference. 6 (pp. 392-396).*

Schwingshackl, C., Petitta, M., Wagner, J. E., Belluardo, G., Moser, D., Castelli, M., Zebisch, M., & Tetzlaff, A. (2013). Wind effect on PV module temperature: Analysis of different techniques for an accurate estimation. *Energy Procedia*, *40*, 77–86. https://doi.org/10.1016/j.egypro.2013.08.010

Servant. (1985). *Calculation of the cell temperature for photovoltaic modules from climatic data. In Intersol Eighty Five (pp. 1640-1643). Pergamon.*

Skoplaki, E., Boudouvis, A. G., & Palyvos, J. A. (2008). A simple correlation for the operating temperature of photovoltaic modules of arbitrary mounting. *Solar Energy Materials and Solar Cells*, *92*(11), 1393–1402. https://doi.org/10.1016/j.solmat.2008.05.016

Stefan Krauter, & Alexander Priess. (2009). *COMPARISON OF MODULE TEMPERATURE MEASUREMENT METHODS, 34th IEEE Photovoltaic Specialists Conference (PVSC), Philadelphia, Pennsylvania, USA, 7-12 June 2009.*

Sulaiman, S. A., Hussain, H. H., Leh, N. S. H. N., & Razali, M. S. (2011). *Effects of dust on the performance of PV panels. World Academy of Science, Engineering and Technology, 58(2011), 588-593.*

Trinuruk, P., Sorapipatana, C., & Chenvidhya, D. (2009). Estimating operating cell temperature of BIPV modules in Thailand. *Renewable Energy*, *34*(11), 2515–2523. https://doi.org/10.1016/j.renene.2009.02.027

# APPENDICES

## A. Nine Thermistor Temperature Sensor Arduino Code

```
int decimalPrecision = 2;

float BValue = 3950;

float R = 10000;

float T = 298.15;

float voltageDividerR = 10000;


int Thermistor1Pin = A1;
    float R1 ;
    float T1 ;
    float a1 ;
    float b1 ;
    float c1 ;
    float d1 ;
    float e1 = 2.718281828 ;
    float tempSampleRead1  = 0;
    float tempLastSample1  = 0;
    float tempSampleSum1   = 0;
    float tempSampleCount1 = 0;
    float tempMean1 ;
```

```
int Thermistor2Pin = A2;
float R2 ;
float T2 ;
float a2 ;
float b2 ;
float c2 ;
float d2 ;
float e2 = 2.718281828 ;
float tempSampleRead2  = 0;
float tempLastSample2  = 0;
float tempSampleSum2   = 0;
float tempSampleCount2 = 0;
float tempMean2 ;

int Thermistor3Pin = A3;
float R3 ;
float T3 ;
float a3 ;
float b3 ;
float c3 ;
float d3 ;
```

```
float e3 = 2.718281828 ;
float tempSampleRead3  = 0;
float tempLastSample3  = 0;
float tempSampleSum3   = 0;
float tempSampleCount3 = 0;
float tempMean3 ;

int Thermistor4Pin = A4;
float R4 ;
float T4 ;
float a4 ;
float b4 ;
float c4 ;
float d4 ;
float e4 = 2.718281828 ;
float tempSampleRead4  = 0;
float tempLastSample4  = 0;
float tempSampleSum4   = 0;
float tempSampleCount4 = 0;
float tempMean4 ;

int Thermistor5Pin = A5;
```

```
float R5 ;

float T5 ;

float a5 ;

float b5 ;

float c5 ;

float d5 ;

float e5 = 2.718281828 ;

float tempSampleRead5  = 0;

float tempLastSample5  = 0;

float tempSampleSum5   = 0;

float tempSampleCount5 = 0;

float tempMean5 ;


int Thermistor6Pin = A6;

float R6 ;

float T6 ;

float a6 ;

float b6 ;

float c6 ;

float d6 ;

float e6 = 2.718281828 ;

float tempSampleRead6  = 0;
```

```
float tempLastSample6  = 0;
float tempSampleSum6   = 0;
float tempSampleCount6 = 0;
float tempMean6 ;

int Thermistor7Pin = A7;
float R7 ;
float T7 ;
float a7 ;
float b7 ;
float c7 ;
float d7 ;
float e7 = 2.718281828 ;
float tempSampleRead7  = 0;
float tempLastSample7  = 0;
float tempSampleSum7   = 0;
float tempSampleCount7 = 0;
float tempMean7 ;

int Thermistor8Pin = A8;
float R8 ;
float T8 ;
```

```
float a8 ;

float b8 ;

float c8 ;

float d8 ;

float e8 = 2.718281828 ;

float tempSampleRead8  = 0;

float tempLastSample8  = 0;

float tempSampleSum8   = 0;

float tempSampleCount8 = 0;

float tempMean8 ;


int Thermistor9Pin = A9;

float R9 ;

float T9 ;

float a9 ;

float b9 ;

float c9 ;

float d9 ;

float e9 = 2.718281828 ;

float tempSampleRead9  = 0;

float tempLastSample9  = 0;

float tempSampleSum9   = 0;
```

```
    float tempSampleCount9 = 0;
    float tempMean9 ;

void setup()
{
    Serial.begin(9600);
}

void loop()

{

    if(millis() >= tempLastSample1 + 1)
        {
            tempSampleRead1 = analogRead(Thermistor1Pin);
            tempSampleSum1 = tempSampleSum1+tempSampleRead1;
            tempSampleCount1 = tempSampleCount1+1;
            tempLastSample1 = millis();
        }

    if(tempSampleCount1 == 1000)
        {
```

```
        tempMean1 = tempSampleSum1 / tempSampleCount1;
        R1 = (voltageDividerR*tempMean1)/(1023-tempMean1);

        a1 = 1/T;
        b1 = log10(R/R1);
        c1 = b1 / log10(e1);
        d1 = c1 / BValue ;
        T1 = 1 / (a1- d1);

        Serial.print("Temperature 1: ");
        Serial.print(T1 - 273.15,decimalPrecision);
        Serial.println(" °C");

        tempSampleSum1 = 0;
        tempSampleCount1 = 0;
    }

if(millis() >= tempLastSample2 + 1)
    {
        tempSampleRead2 = analogRead(Thermistor2Pin);
        tempSampleSum2 = tempSampleSum2+tempSampleRead2;
        tempSampleCount2 = tempSampleCount2+1;
```

```
    tempLastSample2 = millis();
  }

if(tempSampleCount2 == 1000)
  {
    tempMean2 = tempSampleSum2 / tempSampleCount2;
    R2 = (voltageDividerR*tempMean2)/(1023-tempMean2);

    a2 = 1/T;
    b2 = log10(R/R2);
    c2 = b2 / log10(e2);
    d2 = c2 / BValue ;
    T2 = 1 / (a2- d2);

    Serial.print("Temperature 2: ");
    Serial.print(T2 - 273.15,decimalPrecision);
    Serial.println(" °C");

    tempSampleSum2 = 0;
    tempSampleCount2 = 0;
  }
```

```
if(millis() >= tempLastSample3 + 1)
  {
    tempSampleRead3 = analogRead(Thermistor3Pin);
    tempSampleSum3 = tempSampleSum3+tempSampleRead3;
    tempSampleCount3 = tempSampleCount3+1;
    tempLastSample3 = millis();
  }

if(tempSampleCount3 == 1000)
  {
    tempMean3 = tempSampleSum3 / tempSampleCount3;
    R3 = (voltageDividerR*tempMean3)/(1023-tempMean3);

    a3 = 1/T;
    b3 = log10(R/R3);
    c3 = b3 / log10(e3);
    d3 = c3 / BValue ;
    T3 = 1 / (a3- d3);

    Serial.print("Temperature 3: ");
    Serial.print(T3 - 273.15,decimalPrecision);
    Serial.println(" °C");
```

```
    tempSampleSum3 = 0;
    tempSampleCount3 = 0;
  }

if(millis() >= tempLastSample4 + 1)
  {
    tempSampleRead4 = analogRead(Thermistor4Pin);
    tempSampleSum4 = tempSampleSum4+tempSampleRead4;
    tempSampleCount4 = tempSampleCount4+1;
    tempLastSample4 = millis();
  }

if(tempSampleCount4 == 1000)
  {
    tempMean4 = tempSampleSum4 / tempSampleCount4;
    R4 = (voltageDividerR*tempMean4)/(1023-tempMean4);

    a4 = 1/T;
    b4 = log10(R/R4);
    c4 = b4 / log10(e4);
    d4 = c4 / BValue ;
```

```
    T4 = 1 / (a4- d4);

    Serial.print("Temperature 4: ");
    Serial.print(T4 - 273.15,decimalPrecision);
    Serial.println(" °C");

    tempSampleSum4 = 0;
    tempSampleCount4 = 0;
  }

if(millis() >= tempLastSample5 + 1)
  {
    tempSampleRead5 = analogRead(Thermistor5Pin);
    tempSampleSum5 = tempSampleSum5+tempSampleRead5;
    tempSampleCount5 = tempSampleCount5+1;
    tempLastSample5 = millis();
  }

if(tempSampleCount5 == 1000)
  {
    tempMean5 = tempSampleSum5 / tempSampleCount5;
    R5 = (voltageDividerR*tempMean5)/(1023-tempMean5);
```

```
    a5 = 1/T;
    b5 = log10(R/R5);
    c5 = b5 / log10(e5);
    d5 = c5 / BValue ;
    T5 = 1 / (a5- d5);

    Serial.print("Temperature 5: ");
    Serial.print(T5 - 273.15,decimalPrecision);
    Serial.println(" °C");

    tempSampleSum5 = 0;
    tempSampleCount5 = 0;
  }

if(millis() >= tempLastSample6 + 1)
  {
    tempSampleRead6 = analogRead(Thermistor6Pin);
    tempSampleSum6 = tempSampleSum6+tempSampleRead6;
    tempSampleCount6 = tempSampleCount6+1;
    tempLastSample6 = millis();
  }
```

```
if(tempSampleCount6 == 1000)
  {
     tempMean6 = tempSampleSum6 / tempSampleCount6;
     R6 = (voltageDividerR*tempMean6)/(1023-tempMean6);

     a6 = 1/T;
     b6 = log10(R/R6);
     c6 = b6 / log10(e6);
     d6 = c6 / BValue ;
     T6 = 1 / (a6- d6);

     Serial.print("Temperature 6: ");
     Serial.print(T6 - 273.15,decimalPrecision);
     Serial.println(" °C");

     tempSampleSum6 = 0;
     tempSampleCount6 = 0;
  }

if(millis() >= tempLastSample7 + 1)
  {
```

```
    tempSampleRead7 = analogRead(Thermistor7Pin);
    tempSampleSum7 = tempSampleSum7+tempSampleRead7;
    tempSampleCount7 = tempSampleCount7+1;
    tempLastSample7 = millis();
  }

if(tempSampleCount7 == 1000)
  {
    tempMean7 = tempSampleSum7 / tempSampleCount7;
    R7 = (voltageDividerR*tempMean7)/(1023-tempMean7);

    a7 = 1/T;
    b7 = log10(R/R7);
    c7 = b7 / log10(e7);
    d7 = c7 / BValue ;
    T7 = 1 / (a7- d7);

    Serial.print("Temperature 7: ");
    Serial.print(T7 - 273.15,decimalPrecision);
    Serial.println(" °C");

    tempSampleSum7 = 0;
```

```
    tempSampleCount7 = 0;
  }

if(millis() >= tempLastSample8 + 1)
  {
    tempSampleRead8 = analogRead(Thermistor8Pin);
    tempSampleSum8 = tempSampleSum8+tempSampleRead8;
    tempSampleCount8 = tempSampleCount8+1;
    tempLastSample8 = millis();
  }

if(tempSampleCount8 == 1000)
  {
    tempMean8 = tempSampleSum8 / tempSampleCount8;
    R8 = (voltageDividerR*tempMean8)/(1023-tempMean8);

    a8 = 1/T;
    b8 = log10(R/R8);
    c8 = b8 / log10(e8);
    d8 = c8 / BValue ;
    T8 = 1 / (a8- d8);
    Serial.print("Temperature 8: ");
```

```
    Serial.print(T8 - 273.15,decimalPrecision);
    Serial.println(" °C");

    tempSampleSum8 = 0;
    tempSampleCount8 = 0;
  }

if(millis() >= tempLastSample9 + 1)
  {
    tempSampleRead9 = analogRead(Thermistor9Pin);
    tempSampleSum9 = tempSampleSum9+tempSampleRead9;
    tempSampleCount9 = tempSampleCount9+1;
    tempLastSample9 = millis();
  }

if(tempSampleCount9 == 1000)
  {
    tempMean9 = tempSampleSum9 / tempSampleCount9;
    R9 = (voltageDividerR*tempMean9)/(1023-tempMean9);

    a9 = 1/T;
    b9 = log10(R/R9);
```

```
        c9 = b9 / log10(e9);
        d9 = c9 / BValue ;
        T9 = 1 / (a9- d9);

        Serial.print("Temperature 9: ");
        Serial.print(T9 - 273.15,decimalPrecision);
        Serial.println(" °C");

        tempSampleSum9 = 0;
        tempSampleCount9 = 0;
    }
}
```

## B. Thermistor Output Table

### 10K-2 Thermistor Output Table

| °F | °C | Ohms |
|---|---|---|
| -39 | -39.44 | 323839 |
| -37 | -38.33 | 300974 |
| -35 | -37.22 | 279880 |
| -33 | -36.11 | 260410 |
| -31 | -35.00 | 242427 |
| -29 | -33.89 | 225809 |
| -27 | -32.78 | 210443 |
| -25 | -31.67 | 196227 |
| -23 | -30.56 | 183068 |
| -21 | -29.44 | 170775 |
| -19 | -28.33 | 159488 |
| -17 | -27.22 | 149024 |
| -15 | -26.11 | 139316 |
| -13 | -25.00 | 130306 |
| -11 | -23.89 | 121939 |
| -9 | -22.78 | 114165 |
| -7 | -21.67 | 106939 |
| -5 | -20.56 | 100218 |
| -3 | -19.44 | 93909 |
| -1 | -18.33 | 88090 |
| 1 | -17.22 | 82670 |
| 3 | -16.11 | 77620 |
| 5 | -15.00 | 72911 |
| 7 | -13.89 | 68518 |
| 9 | -12.78 | 64419 |
| 11 | -11.67 | 60592 |
| 13 | -10.56 | 57017 |
| 15 | -9.44 | 53647 |
| 17 | -8.33 | 50526 |
| 19 | -7.22 | 47606 |
| 21 | -6.11 | 44874 |
| 23 | -5.00 | 42317 |
| 25 | -3.89 | 39921 |
| 27 | -2.78 | 37676 |
| 29 | -1.67 | 35573 |
| 31 | -0.56 | 33599 |
| 33 | 0.56 | 31732 |
| 35 | 1.67 | 29996 |
| 37 | 2.78 | 28365 |
| 39 | 3.89 | 26834 |
| 41 | 5.00 | 25395 |
| 43 | 6.11 | 24042 |
| 45 | 7.22 | 22770 |
| 47 | 8.33 | 21573 |
| 49 | 9.44 | 20446 |
| 51 | 10.56 | 19376 |
| 53 | 11.67 | 18378 |
| 55 | 12.78 | 17437 |
| 57 | 13.89 | 16550 |
| 59 | 15.00 | 15714 |
| 61 | 16.11 | 14925 |
| 63 | 17.22 | 14180 |
| 65 | 18.33 | 13478 |
| 67 | 19.44 | 12814 |
| 69 | 20.56 | 12182 |
| 71 | 21.67 | 11590 |
| 73 | 22.78 | 11030 |
| 75 | 23.89 | 10501 |
| 77 | 25.00 | 10000 |
| 79 | 26.11 | 9526 |
| 81 | 27.22 | 9078 |
| 83 | 28.33 | 8653 |
| 85 | 29.44 | 8251 |
| 87 | 30.56 | 7866 |
| 89 | 31.67 | 7505 |
| 91 | 32.78 | 7163 |
| 93 | 33.89 | 6838 |
| 95 | 35.00 | 6530 |
| 97 | 36.11 | 6238 |
| 99 | 37.22 | 5960 |
| 101 | 38.33 | 5697 |
| 103 | 39.44 | 5447 |
| 105 | 40.56 | 5207 |
| 107 | 41.67 | 4981 |
| 109 | 42.78 | 4766 |
| 111 | 43.89 | 4561 |
| 113 | 45.00 | 4367 |
| 115 | 46.11 | 4182 |
| 117 | 47.22 | 4006 |
| 119 | 48.33 | 3838 |
| 121 | 49.44 | 3679 |
| 123 | 50.56 | 3525 |
| 125 | 51.67 | 3380 |
| 127 | 52.78 | 3242 |
| 129 | 53.89 | 3111 |
| 131 | 55.00 | 2985 |
| 133 | 56.11 | 2865 |
| 135 | 57.22 | 2751 |
| 137 | 58.33 | 2642 |
| 139 | 59.44 | 2538 |
| 141 | 60.56 | 2438 |
| 143 | 61.67 | 2343 |
| 145 | 62.78 | 2252 |
| 147 | 63.89 | 2165 |
| 149 | 65.00 | 2082 |
| 151 | 66.11 | 2003 |
| 153 | 67.22 | 1927 |
| 155 | 68.33 | 1855 |
| 157 | 69.44 | 1785 |
| 159 | 70.56 | 1718 |
| 161 | 71.67 | 1655 |
| 163 | 72.78 | 1594 |
| 165 | 73.89 | 1536 |
| 167 | 75.00 | 1480 |
| 169 | 76.11 | 1427 |
| 171 | 77.22 | 1375 |
| 173 | 78.33 | 1326 |
| 175 | 79.44 | 1279 |
| 177 | 80.56 | 1234 |
| 179 | 81.67 | 1190 |
| 181 | 82.78 | 1149 |
| 183 | 83.89 | 1109 |
| 185 | 85.00 | 1070 |
| 187 | 86.11 | 1034 |

## C. PV Module Specifications

| PV Module Specs | |
|---|---|
| $\eta_{PV,ref}$ | **0.1070** |
| Area ($m^2$) | **0.34** |
| Peak Power (W) | **40** |
| $G_{STC}$ ($W/m^2$) | **1000** |
| $T_{STC}$ ($^oC$) | **25** |
| NOCT ($^oC$) | **45** |
| $G_{ref, NOCT}$ ($W/m^2$) | **800** |
| $T_{ref, NOCT}$ ($^oC$) | **20** |
| $\beta_{ref}$ (1/K) | **0.004** |

**TEZ İZİN FORMU** / THESIS PERMISSION FORM

**PROGRAM** / PROGRAM

| | |
|---|---|
| Sürdürülebilir Çevre ve Enerji Sistemleri / Sustainable Environment and Energy Systems | ☑ |
| Siyaset Bilimi ve Uluslararası İlişkiler / Political Science and International Relations | ☐ |
| İngilizce Öğretmenliği / English Language Teaching | ☐ |
| Elektrik Elektronik Mühendisliği / Electrical and Electronics Engineering | ☐ |
| Bilgisayar Mühendisliği / Computer Engineering | ☐ |
| Makina Mühendisliği / Mechanical Engineering | ☐ |

**YAZARIN** / AUTHOR
**Soyadı** / Surname : Youssef
**Adı** / Name : Youssef Maged Mohamed Baligh
**Programı** / Program : Sustainable Environment Energy Systems

**TEZİN ADI** / TITLE OF THE THESIS (**İngilizce** / English) :
PV CELL TEMPERATURE ESTIMATION AND PERFORMANCE ANALYSIS BASED ON CHANGING ENVIRONMENTAL EFFECTS

**TEZİN TÜRÜ** / DEGREE: **Yüksek Lisans** / Master ☑ **Doktora** / PhD ☐

1. **Tezin tamamı dünya çapında erişime açılacaktır.** / Release the entire work immediately for access worldwide. ☐

2. **Tez <u>iki yıl</u> süreyle erişime kapalı olacaktır.** / Secure the entire work for patent and/or proprietary purposes for a period of **<u>two years</u>**. * ☑

3. **Tez <u>altı ay</u> süreyle erişime kapalı olacaktır.** / Secure the entire work for period of **<u>six months</u>**. * ☐

**Yazarın imzası** / Author Signature ..... **Tarih** / Date 4/10/2022

**Tez Danışmanı** / Thesis Advisor Full Name: Asst Prof Canras Batunlu

**Tez Danışmanı İmzası** / Thesis Advisor Signature: .....

**Eş Danışmanı** / Co-Advisor Full Name: —

**Eş Danışmanı İmzası** / Co-Advisor Signature: —

**Program Koordinatörü** / Program Coordinator Full Name: Assoc Prof Ceren İnce Derogar

**Program Koordinatörü İmzası** / Program Coordinator Signature: .....